NEANDC (E)-262 U Vol. V
INDC (Ger)-28/LN + Special

PROGRESS REPORT ON NUCLEAR DATA RESEARCH IN THE FEDERAL REPUBLIC OF GERMANY

for the Period April 1, 1984 to March 31, 1985

June 1985

Edited by
S.M. Qaim

Institut für Chemie (1): Nuklearchemie
Kernforschungsanlage Jülich GmbH

NEANDC (E)-262 U Vol. V
INDC (Ger)-28/LN + Special

PROGRESS REPORT ON NUCLEAR DATA RESEARCH IN THE FEDERAL REPUBLIC OF GERMANY

for the Period April 1, 1984 to March 31, 1985

June 1985

Edited by
S.M. Qaim

Institut für Chemie (1): Nuklearchemie
Kernforschungsanlage Jülich GmbH

F O R E W O R D

This report has been prepared to promote exchange of nuclear data research information between the Federal Republic of Germany and other member states of NEA and IAEA. It brings together progress reports from KfK Karlsruhe, KFA Jülich, GKSS-Geesthacht, the Universities of Kiel, Köln, Mainz, Marburg, Stuttgart and München, as well as from PTB Braunschweig and FIZ Karlsruhe. An in previous years, the emphasis in the work reported here has been on measurement, evaluation and compilation of application oriented nuclear data, such as those relevant to fission and fusion reactor technologies, development of intense spallation neutron sources, production of medically important short-lived radio-isotopes etc.

Each contribution is presented under the laboratory heading where the work was done. If the work is relevant to requests in the World Request List for Nuclear Data, WRENDA 83/84 (INDC(SEC)-88/URSF), the corresponding request identification numbers have been listed after the title and authors' names of the respective contribution.

Jülich, June 1985 S.M. Qaim

C O N T E N T S

Page

Page

PHYSIKALISCH-TECHNISCHE BUNDESANSTALT

BRAUNSCHWEIG

KERNFORSCHUNGSZENTRUM KARLSRUHE
INSTITUT FÜR KERNPHYSIK II

1. Systematics of Angular-Dependent Neutron Production by 585 MeV Protons on Targets with $12 \leq A \leq 238$

S. Cierjacks, Y. Hino[1], F. Raupp, S.D. Howe[2], L. Buth[3]

In continuation of our experimental studies on neutron production from high-energy proton bombardment of thin metal targets [1] the systematic results have been compared with previous measurements of differential (p,n´)- and (p,p´)-cross sections. Furthermore, these data have been discussed and explained in terms of the relevant types of nucleon-nucleus reaction mechanisms. Since angular distributions in the laboratory coordinate system often do not reveal the true angular dependence of nucleon-nucleus interactions, the data have been converted to the zero-linear-momentum (ZLM) coordinate system of the incident proton and the target nucleus. On this basis the observed differences in the evaporation spectra for different angles could be attributed to the recoil-nucleus motion, and thus are not inconsistent with an expected isotropy or a 90°-symmetry in the ZLM system. In the cascade region the differential neutron data revealed a similar behavior as the corresponding (p,p´)-data. The most obvious differences refer to the absolute values of the cross sections wich are in the heavier element region significantly higher for (p,n´)- than for (p,p´)-data. The ratios of comparable neutron and proton data seem to be of the order of the ratios of neutrons to protons in the corresponding target nuclei.

2. Validation of Intranuclear -Cascade-Evaporation-Model Calculations for Proton-Induced Neutron Production

S. Cierjacks, Y. Hino[1], D. Filges[4], T.W. Armstrong[4], P. Cloth[4]

As part of a study to asses the accuracy of model predictions from theory the intranuclear cascade-evaporation model in its version of HETC/KFA-1 [2] has been used to calculate differential neutron production cross sections for 590 MeV protons on uranium, lead, tantalum, indium, niobium, iron, aluminum

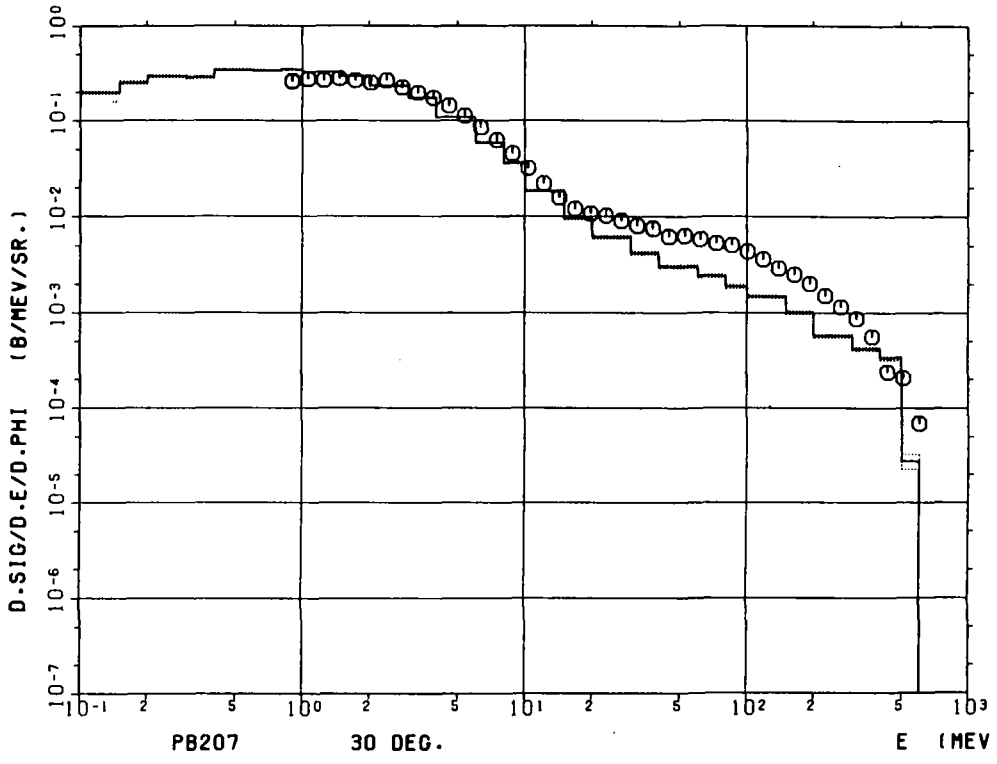

Fig. 1 Measured (ϕ) and calculated (—) 30° neutron production cross sections for 590 MeV protons on lead. It can be seen that the HETC/KFA-1 code predicts approximately the correct cross section in the evaporation region ($E_n \lesssim 15$ MeV), whereas in the cascade region ($E_n \gtrsim 15$ MeV) there are systematic discrepancies.

and carbon. These model predictions have been used for comparisons with the systematic KfK-measurements for these targets performed in recent years at the SIN cyclotron [1]. A typical result is given in Fig. 1 which shows the comparison for lead at a laboratory angle of 30°. In general, the HETC/KFA-1 code predicts within ∿ 20% the cross section in the evaporation region ($E_n \lesssim 15$ MeV) for all target nuclei except the very lightest, aluminum and carbon. For the latter some larger deviations exist. A major deficiency of the existing HETC code is the underestimation of high-energy neutron production ($E_n \gtrsim 15$ MeV). As can be judged from Fig. 1 the calculations yield 30° cross sections which are at ∿ 100 MeV by a factor of 2-3 smaller than the measured ones. The underestimation of high-energy neutrons further increases with increasing emission angle and increasing emission energy [3]. The different possibilities for suitable model modifications which can improve the agreement between measurements and calculations are presently under discussion. A detailed comparison of all measured and calculated cross sections has been published in a joint KfK/KFA report [4].

3. A Large-Area Position-Sensitive Time-of-Flight Counter for Energetic Neutrons and Charged Particles

S. Cierjacks, T. Petković[5], H. Ullrich, D. Gotta, S. Ljungfelt, N. Šimičević[5], M. Izycki[6], P. Weber[6], H.J. Weyer[6]

A large position-sensitive scintillation counter has been designed for neutron and charged-particle detection in the range from about 10 to 300 MeV [5]. The time-of-flight counter consists of thirty bars of 5x10 cm^2 cross section, each 2 m in length, arranged in a suitable counter matrix covering an overall effective detection area of $\sim$ 1x2 m^2. The individual bars have pulse-height responses over the length uniform to 5% except close to the ends, position resolutions of almost 5 cm and intrinsic time dispersions of 450 ps. Typical integral neutron detection efficiencies are 19% for 50 MeV neutrons and 13% for 170 MeV neutrons at a pulse height threshold of 5 MeV electron-equivalent energy.

---

[1] Now at Radiation & Radioactivity Metrology Section, Electrotechnical Laboratory, Umezono, Ibaraki, Japan

[2] Now at Los Alamos National Laboratory, Los Alamos, New Mexico, USA

[3] Permanent member of the Institut für Neutronenphysik und Reaktortechnik, Kernforschungszentrum Karlsruhe

[4] Institut für Reaktorentwicklung, Kernforschungsanlage Jülich, Jülich, Fed. Rep. of Germany

[5] On leave from University of Zagreb, Zagreb, Yugoslavia

[6] Institute of Physics, University of Basel, Basel, Switzerland

References

[1] S. Cierjacks, Y. Hino, S.D. Howe, F. Raupp and L. Buth, Differential Neutron Production Cross Sections for 590 MeV Protons, Proc. Intern. Conf. on Nuclear Data for Science and Technology, Antwerp, 1982, (D. Reidel Publ. Comp., Dordrecht, 1983) p.383

[2] P. Cloth, D. Filges, G. Sterzenbach, T.W. Armstrong and B.L. Colborn, The KFA-Version of the High-Energy Transport Code HETC and the Generalized Evaluation Code SIMPEL, Kernforschungsanlage Jülich Report, Jül-Spez-196, March 1983

[3] S. Cierjacks, Y. Hino, D. Filges, T.W. Armstrong and P. Cloth, Validation of HETC Model Calculations for Neutron Production, Ann. Report on Nuclear Physics Activities July 1, 1983 - June 30, 1984, Eds. D.C. Fries, P. Matussek, Ch. Weddigen, Kernforschungszentrum Karlsruhe Report, KfK 3815, Oct. 1984, p. 103

[4] D. Filges, S. Cierjacks, Y. Hino, T.W. Armstrong and P. Cloth, Validation of the Intranuclear Cascade-Evaporation Model for Particle Production, Joint KfK/KFA Report, Jül-1960, KfK 3779, Nov. 1984

[5] S. Cierjacks, T. Petković, H. Ullrich, D. Gotta, S. Ljungfelt, N. Šimičević, M. Izycki, P. Weber, H.J. Weyer, A Large-Area Position-Sensitive Time-of-Flight Counter for Energetic Neutrons and Charged Particles, Nucl. Instr. and Meth., in press

KERNFORSCHUNGSZENTRUM KARLSRUHE
INSTITUT FÜR KERNPHYSIK III

1. 3 MV Van de Graaff-Accelerator

1.1 The ^{26}Al (n,p)-Reaction

H.P. Trautvetter[+], H.W. Becker[+], U. Heinemann[+], C. Rolfs[+], F. Käppeler, P. Geltenbort[++], F. Gönnenwein[++], M. Baumann[+++], H. Freiesleben[+++]

The cosmologically short lived isotope ^{26}Al ($t_{1/2}$ = 7.2•10^5 y) might be useful as a clock for the early solar system. The discovery of an excess of ^{26}Mg in the meteorite Allende indicates that this is due to the decay of ^{26}Al which eventually was produced by a nearby nova or supernova shortly before the solar system formed. The ^{26}Al(n,p) reaction is important as it influences the destruction rate of this isotope in a neutron rich environment.

We have measured the (n,p) cross section at thermal neutron energies and in the keV region, using neutron spectra which closely resembled the true Maxwellian distributions for kT = 31 and kT = 71 keV. An additional measurement was made at E_n = 310 ± 40 keV. The experimental setup is shown in Fig. 1. Protons are detected by a ΔE,E-telescope consisting of thin silicon surface barrier detectors to minimize backgrounds from gamma-rays and neutron induced events in the detectors. The samples had an area of 616 mm² and a thickness of 1.5 - 2.4•10^{15} atoms/cm² [1].

The reaction may proceed via the ground state of ^{26}Mg or via the 5 first excited states. The respective proton groups p_0 to p_5 are to be expected with different intensity because of different centrifugal barriers. In our measurements we succeeded to detect the most intense p_1-group and also the p_0-group quantitatively. The higher groups were too low in energy and could not be discriminated from the background (except p_2 at thermal energies, where backgrounds were not so severe). The results are summarized in Table I and are plotted in Fig. 2

+ University of Münster, D-4400 Münster, Federal Republic of Germany
++ Institut Laue-Langevin, Grenoble, France
+++ University of Bochum, D-4630 Bochum, Federal Republic of Germany

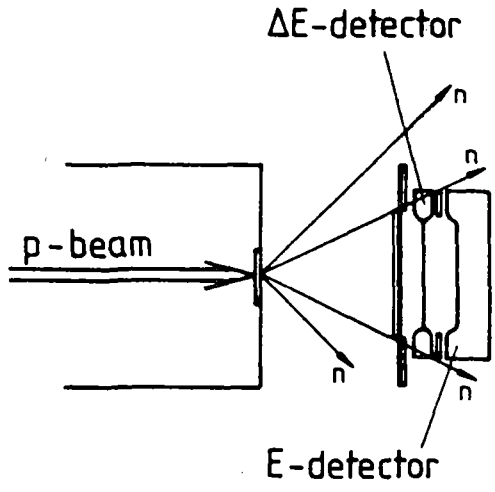

Fig. 1 Experimental setup used at the Van de Graaff (top) and at the ILL reactor (bottom).

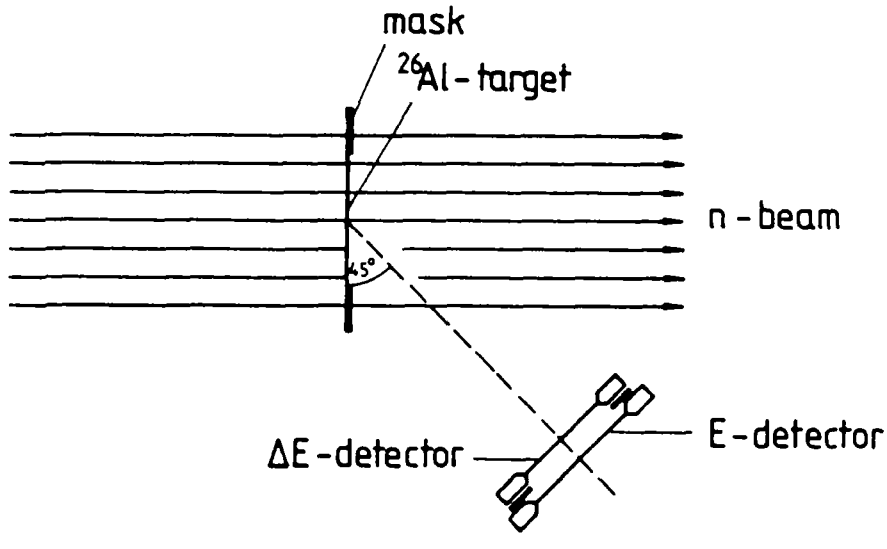

Table I Experimental Cross Sections for the ^{26}Al (n,p) Reaction

		ILL-Reactor	Van de Graaff accelerator		
E_n(keV)		$40 \cdot 10^{-6}$	kT=31	kT=71	310±40[a]
(n,p)-Cross Section (mb)	P_0	26±10	13+6	-	21±8
	P_1	1850±150	124±13	84±14	72±16
	P_2	185	-	-	-

[a] Neutron spectrum ranging from 270 to 350 keV.

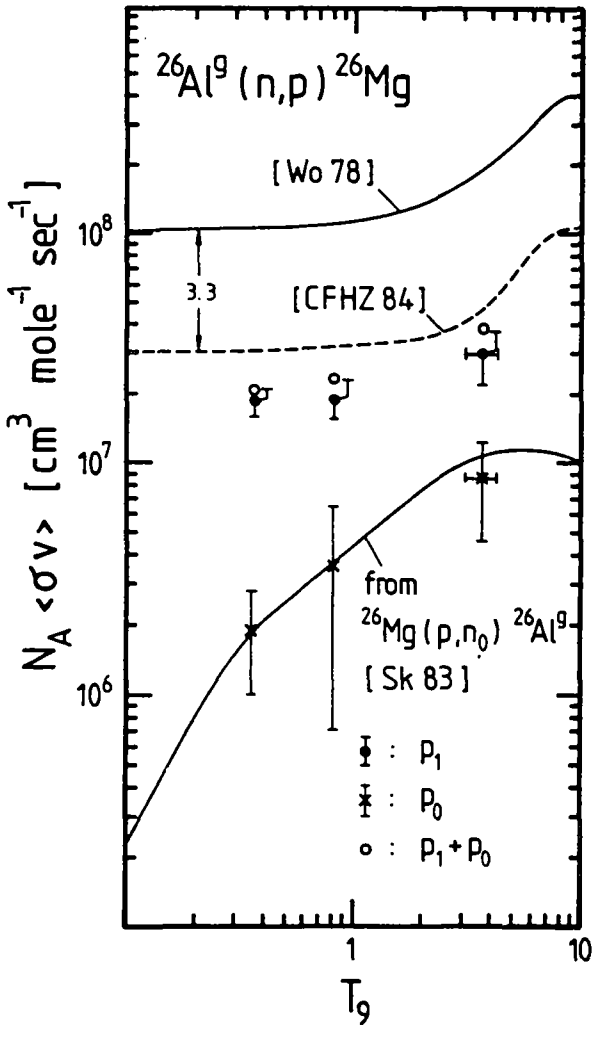

Fig. 2 Comparison of the experimental reaction rates $N_A\langle\sigma v\rangle = N_A\bar{\sigma}v_T$, ($N_A$ = Avogadros number, v_T = mean thermal velocity) with those deduced for the p_0 group from the inverse reaction [2] and with theoretical calculations [3,4].

References

[1] L. Buchmann, H. Baumeister, C. Rolfs, Nucl. Instr. Meth., in press

[2] R.T. Skelton, R.W. Kavanagh, D.G. Sargood, Ap. J. 271 (1983) 404

[3] S.E. Woosley, W.A. Fowler, J.A. Holmes, B. Zimmerman, Atomic Data and Nuclear Data Tables 22 (1978) 371

[4] G.R. Caughlan, W.A. Fowler, M.J. Harris, B. Zimmerman, Atomic Data and Nuclear Data Tables (1985), in press

1.2 Stellar Neutron Capture Rates for ^{46}Ca and ^{48}Ca*

F. Käppeler, G. Walter, G.J. Mathews+

Stellar neutron capture rates for ^{46}Ca and ^{48}Ca have been measured by the activation technique. Both kT = 25 keV Maxwellian-like incident neutron spectra and non-Maxwellian higher-energy spectra have been utilized to study the pos-

---

* The Astrophysical Journal (in press)

+ University of California, Lawrence Livermore National Laboratory, California 94550, USA

sible role of individual capture resonances. Maxwellian averaged (kT = 30 keV) cross sections are derived for ^{46}Ca and ^{48}Ca (Table I). The possibility of a neutron capture origin for ^{46}Ca and ^{48}Ca is discussed in the light of these new cross sections as well as a mechanism for the production of the observed isotopic anomalies in inclusion EK-1-4-1 from the Allende meteorite.

Table I Experimental Results of the Maxwellian Averaged (n,γ)-Cross Sections for $^{46,48}Ca$ and Comparison with Model Calculations

	Average Capture Cross Section (mb) for kT = 30 keV	
	^{46}Ca	^{48}Ca
This work (experimental)	5.7 ± 0.5	0.95 ± 0.09
Ref. [1] (calculated)	3.7	1.1

[1] S.E. Woosley, W.A. Fowler, J.A. Holmes, and B.A. Zimmerman, Atomic Data and Nuclear Data Tables 22 (1978) 371

1.3 Measurement of Neutron Capture Cross Sections of s-Only Isotopes: ^{70}Ge, ^{86}Sr, and ^{87}Sr*

G. Walter, H. Beer

In order to improve the s-process data base in the mass range A < 100 the neutron capture cross sections of ^{86}Sr, ^{87}Sr and, for the first time, ^{70}Ge have been measured by time-of-flight in the energy range from 3.5 to 240 keV. The Maxwellian averaged capture cross sections have been calculated from the data for kT = 20 keV up to kT = 50 keV. At kT = 30 keV we obtained the values 92±5, 74±5, and 100±7 mb for ^{70}Ge, ^{86}Sr, and ^{87}Sr, respectively.

* Astron. Astrophys. 142 (1985) 268-272

1.4 keV-Neutron Capture Cross Sections of the Krypton Isotopes*

G. Walter, B. Leugers, F. Käppeler, G. Reffo+, F. Fabbri+

The neutron capture cross sections of the stable krypton isotopes were determined in the energy interval from 4 to 250 keV using a C_6D_6-detector system in conjunction with the time-of-flight technique. The energy resolution of the measurement was 4% at 20 and 6% at 100 keV, and the experimental uncertainties were typically 6 to 10%. The measurements were complemented by statistical model calculations of all krypton isotopes in the mass range 78<A<86 in order to obtain also reliable cross sections for the unstable nuclei ^{79,81,85}Kr. These calculations were based on local systematics for all relevant parameters, and the results were estimated to show uncertainties of 20-25%. Maxwellian average cross sections were calculated for kT=30 keV and are compared with previous work in Table I.

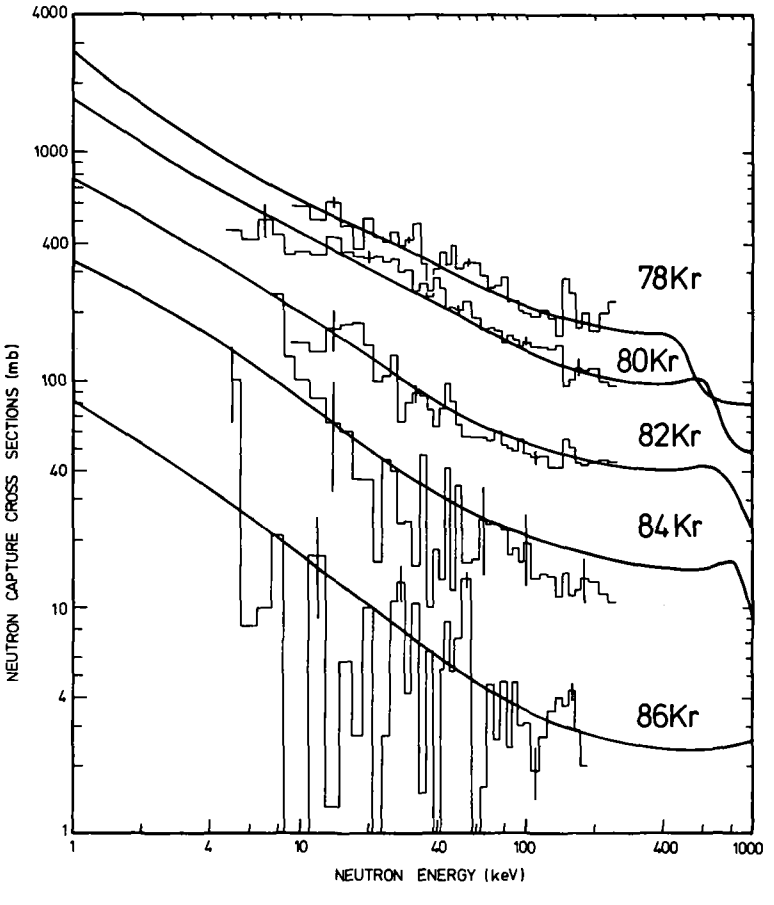

Fig. 1 The averaged experimental cross section (histogram) together with the calculated values (solid line) for the even Kr-isotopes.

---

* submitted to Nuclear Science and Engineering

+ Laboratorio Dati Nucleari, E.N.E.A., Bologna, Italy

Table I Maxwellian Average Neutron Capture Cross Sections for kT = 30 keV: Comparison of Present Theoretical and Experimental Values with Previous Results

Target Isotope	Maxwellian Average Cross Section (mb) for kT = 30 keV				
	Holmes et al.[1]	Leugers et al.[2]	Harris [3]	This Work calc	This Work exp
^{78}Kr	203	284	253	368	359±44
^{79}Kr	1130	-	-	857	-
^{80}Kr	148	228	156	242	257±15
^{81}Kr	1030	800	994	682	-
^{82}Kr	122	95	79	100	84±6
^{83}Kr	571	345	259	237	251±16
^{84}Kr	25	30	13	40	36.5±4.5
^{85}Kr	155	68	25	67±17	-
^{86}Kr	44	-	3.7	8.0±2.8	5.6±0.7

[1] J.A. Holmes, S.E. Woosley, W.A. Fowler, B.A. Zimmerman; Atomic Data and Nuclear Data Tables 18 (1976) 305

[2] B. Leugers, F. Käppeler, F. Fabbri, G. Reffo, Nuclear Cross Sections and Technology, NBS Spec. Publ. 594 (1980) p. 857

[3] M.J. Harris, Astr. Space Sci. 77 (1981) 357

1.5 ^{148,150}Sm: A Test for s-Process Nucleosynthesis*

R.R. Winters+, F. Käppeler, K. Wisshak, A. Mengoni, G. Reffo++

We have measured to a precision of ∿4.5% the neutron capture cross sections of ^{148,149,150}Sm over the neutron energy range $4 < E_n < 250$ keV. These data, in conjunction with calculated cross sections for ^{147}Nd and ^{147,148}Pm, are used to establish a set of Maxwellian-averaged cross sections (Table I) useful for investigation of branchings in the s-process of stellar nucleosynthesis. The ratio of the values of the s-process current $\langle\sigma\rangle N_s$ (Maxwellian-averaged neutron cross section times s-process abundance) for the s-only isotopes ^{148,150}Sm is 0.91 ± 0.03 rather than unity as predicted by the local approximation. We interpret this result as due to an s-process branching which partly bypasses ^{148}Sm. Since the beta decay rates at the branching points are expected to be almost independent of temperature, we are able to obtain an estimate of the

s-process neutron density of $n_n = (1.0 \pm 0.4)\ 10^8\ cm^{-3}$. The new results have also served to considerably improve the $\langle\sigma\rangle N_s$-systematics in the mass region $A \sim 145$.

Table I Experimental and Calculated Maxwellian Averaged (n,γ)-Cross Sections for kT = 30 keV in the Mass Region 147<A<151

Experimental (mb)	^{148}Sm 277 ± 13		^{149}Sm 1511 ± 70		^{150}Sm 465 ± 28
Calculated (mb)	^{147}Nd 625	^{147}Pm 1163	^{148}Pm 1542	$^{148}Pm^m$ 2453	^{151}Sm 1932

* submitted to The Astrophysical Journal

\+ Denison University, Granville, Ohio 43023, USA

++ Laboratorio Dati Nucleari, E.N.E.A., Bologna, Italy

1.6 Neutron Capture Cross Sections and Solar Abundances of $^{160,161}Dy$, $^{170,171}Yb$, $^{175,176}Lu$, and $^{176,177}Hf$ for the s-Process Analysis of the Radionuclide ^{176}Lu*

H. Beer, G. Walter, R.L. Macklin+, P.J. Patchett++

The neutron capture cross sections and solar abundances of $^{160,161}Dy$, $^{170,171}Yb$, $^{175,176}Lu$, and $^{176,177}Hf$ have been measured. With this data base s-process studies have been carried out to determine the s-process neutron density and temperature and to investigate the s-process nucleosynthesis of the ^{176}Lu clock. From various branchings the neutron density was found to be $(0.8 - 1.8) \times 10^8$ neutrons per cm³ and the temperature kT to be 18-28 keV. On the basis of the present data, ^{176}Lu proved not to be applicable as a cosmic clock because of the temperature sensitivity of the ^{176}Lu half-life but be used instead as a stellar thermometer. Constraints for the s-process temperature (kT = 20-28 keV) were found to be in good agreement with the investigated branchings.

* Phys. Rev. C30 (1984) 464

\+ Oak Ridge National Laboratory, Oak Ridge, Tennessee 37830, USA

++ Max Planck-Institut für Chemie, D-6500 Mainz, Federal Republic of Germany

1.7 The ^{163}Dy-^{163}Ho Branching: an s-Process Barometer*

H. Beer, G. Walter, R.L. Macklin+

The neutron capture cross sections of ^{163}Dy and ^{164}Er have been measured to analyse the s-process branching at ^{163}Dy - ^{163}Ho. The reproduction of the s-process abundance of ^{164}Er via this branching is sensitive to temperature kT, neutron density, and electron density n_e. The calculations using information from other branchings on kT and the neutron density n_n give constraints for n_e at the site of the s-process.

Table I Sample Characteristics and Maxwellian Averaged Capture Cross Section σ at the Thermal Energy kT = 30 keV

Sample	Diameter (mm)	Weight (mg)	% Isotopic Composition	σ(mb) at kT=30 keV
Dy_2O_3	15	907.39	96.85 ^{163}Dy	1153 ± 44 (VDG) 1130 ± 45 (ORELA)
Er-metal	6	8.30	1.61 ^{164}Er	714 ± 61 (VDG)

* Contribution to the Fifth International Symposium on Capture Gamma-Ray Spectroscopy and Related Topics, Knoxville, TN, Sept. 10-14, 1984

+ Oak Ridge National Laboratory, Oak Ridge, Tennessee 37831, USA

1.8 $^{198,199,200,201,202,204}Hg(n,\gamma)$ Cross Sections and the Termination of s-Process Nucleosynthesis*

H. Beer, R.L. Macklin+

The neutron capture cross sections of $^{198,199,200,201,202,204}Hg(n,\gamma)$ were measured in the energy range 2.6 keV to 500 keV. The average capture cross sections were calculated and fitted in terms of strength functions. Resonance parameters for the observed resonances were determined by a shape analysis. Max-

* accepted for publ. in Phys. Rev. C

+ Oak Ridge National Laboratory, Oak Ridge, Tennessee 37830, USA

wellian averaged capture cross sections were computed for thermal energies kT between 5 and 100 keV. The solar mercury abundance was determined to be 0.34 ± 0.04 relative to Si = 10^6. The termination of s-process nucleosynthesis at lead and bismuth was investigated. The abundances of $^{206,207,208}Pb$ were reproduced introducing a strong fluence component of the s-process in addition to normal s- and r-process nucleosynthesis. The radiogenic ^{207}Pb abundance was determined and the r-process age was calculated via ^{235}U. Using Fowler's exponential model an age $T = 4.6$ Gyr + $\Delta = 17.2 \pm 2.6$ Gyr was obtained.

KERNFORSCHUNGSZENTRUM KARLSRUHE
INSTITUT FÜR NEUTRONENPHYSIK UND REAKTORTECHNIK

1. Nuclear Data Evaluation

1.1 Release of the Nuclear Data Library KEDAK-4

B. Goel, B. Krieg, E. Stein, U. Fischer, H. Jahn, F.H. Fröhner

A new KEDAK version, KEDAK-4 (revised), was released in October, 1984, and sent to the neutron data centres for further distribution. A short summary documentation is given in [1]. The main changes with respect to KEDAK-3 are as follows.

The point data for Cr, Fe and Ni are revised to take into account new thermal cross section data, in particular new scattering lengths [2], and precision measurements of radiation widths for strong s-wave resonances performed by the Karlsruhe Van-de-Graaff group [3]. Point cross sections are given for zero temperature (instead of room temperature as in KEDAK-3). The corresponding Reich-Moore resonance parameters are given separately for the individual isotopes.

^{232}Th is taken over from ENDF/B-IV, except for the unresolved resonance region which has been newly evaluated, and for the resolved resonance region where point data have been newly generated with the Reich-Moore formalism.

^{238}U point data in the resolved resonance region have been newly generated with the Reich-Moore formalism.

New transplutonium evaluations have been added for ^{241}Am, ^{242m}Am, ^{243}Am [4], ^{244}Cm [4, 5], ^{246}Cm [6] and ^{248}Cm [7].

References

[1] B. Goel, B. Krieg, KfK 3838 (1984)

[2] L. Köster, K. Knopf and W. Waschkowski, Z. Physik A287 (1978) 61
L. Köster and H. Rauch, Rept. IAEA-Contract 2517/RB (1981)

[3] K. Wisshak and F. Käppeler, Nucl. Sci. Eng. 77 (1981) 58;
K. Wisshak, F. Käppeler, G. Reffo and F. Fabbri,
Nucl. Sci. Eng. 86 (1984) 168;
K. Wisshak, F. Käppeler, R.L. Macklin, G. Reffo and F. Fabbri;
Nucl. Sci. Eng. 87 (1984) 48

[4] U. Fischer, KfK 2907 (1980);
B. Goel and F.H. Fröhner, Proc. 12th Int. Symp. on Nucl.
Physics, Gaussig 1982, ZfK 491 (1982) p. 180
F.H. Fröhner, B. Goel, U. Fischer and H. Jahn, Proc. Conf. on
Nucl. Data for Sci. and Technol. (K.H. Böckhoff ed.),
Antwerp (1982), p. 211

[5] M. Caner, S. Yiftah, IA-1353 (1979)

[6] M. Caner, Y. Bartal, S. Yiftah, IA-1358 (1980)

[7] M. Caner, S. Yiftah, IA-1383 (1983)

1.2 Nuclear Data for Fusion Applications

B. Goel, B. Krieg, E. Stein, E. Wiegner, U. Fischer, I. Broeders

An evaluation for the $^{7}Li(n,n't)\alpha$ cross section has been reported previously [1]. In 1984 the new data shown in Fig. 1 became available. Swinhoe [2] has recalculated the multiple-scattering correction to earlier Harwell measurements [3]. The new revised data are about 3 to 6 % higher than the original data, but still systematically lower by about 15 % compared to other experimental data and our own evaluation. The data of Takahashi et al. [4] lie almost exactly on our evaluated curve whereas the value of Smith et al. [5] is about 5 % higher than the KEDAK value. Since the uncertainty given by Smith et al. is 5.3 % a revision of our 1981 evaluation was not deemed necessary. Also shown in Fig. 1 is a recent evaluation of Shibata et al. for JENDL-3 [6].

The JENDL-3 curve is lower throughout than the KEDAK curve by about 3 % which may be due to more weight given to the Harwell data.

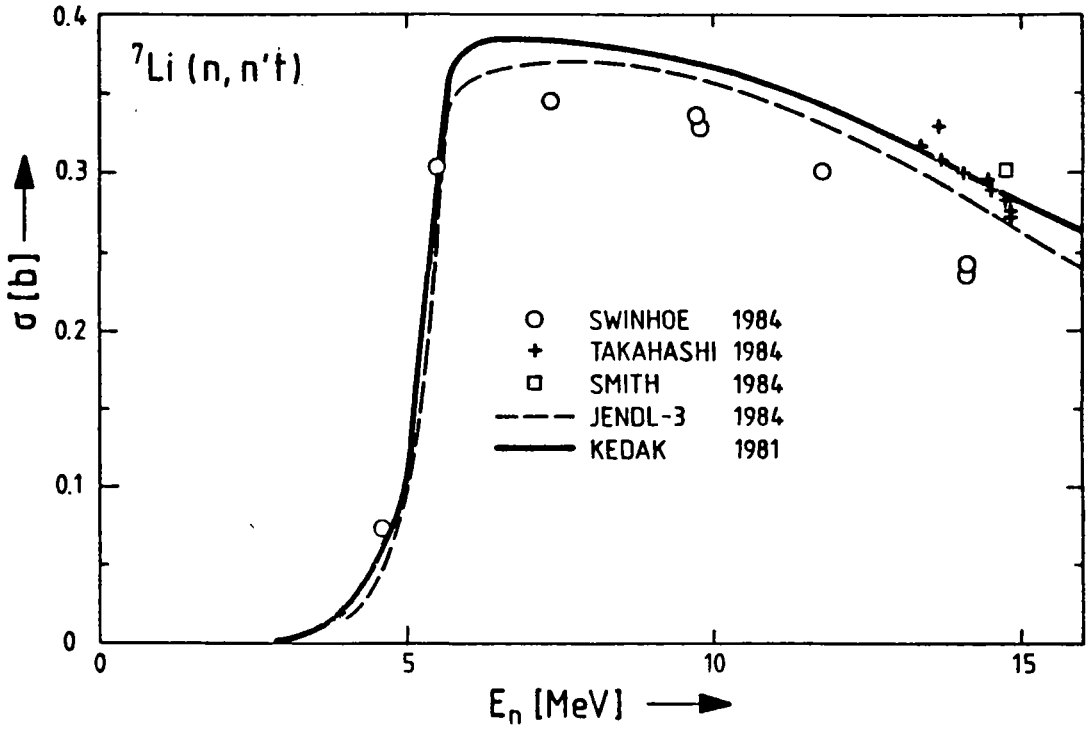

Fig. 1 Recent experimental data and evaluations for the reaction $^7Li(n,n't)\alpha$.

Since ZrH_x is used in some recent fusion blanket designs [7] the heat production rate due to neutron collisions with Zr nuclei is of interest. KERMA factors, defined by $K_x(E) = \sigma_x(E)\ \overline{R}_x(E)$, where $\sigma_x(E)$ and $\overline{R}_x(E)$ are the cross section and the average recoil energy for a neutron of lab energy E causing a reaction of type x, were calculated from the ENDL 82 evaluation in VITAMIN-C group structure [8]. The results for the main reactions are shown in Fig. 2. In order to check data and method KERMA factors calculated for Pb were compared with those available on the MACKLIB-IV library [9]. Agreement was satisfactory for elastic scattering whereas large differences were found for radiative capture. These arise mainly because for capture one has to deal with small differences between similarly large numbers. Moreover, an exact treatment of capture KERMAs requires gamma transport calculations since, in addition to heating by recoiling nuclei, capture gamma rays may deposit energy far away from the place of the capture reaction.

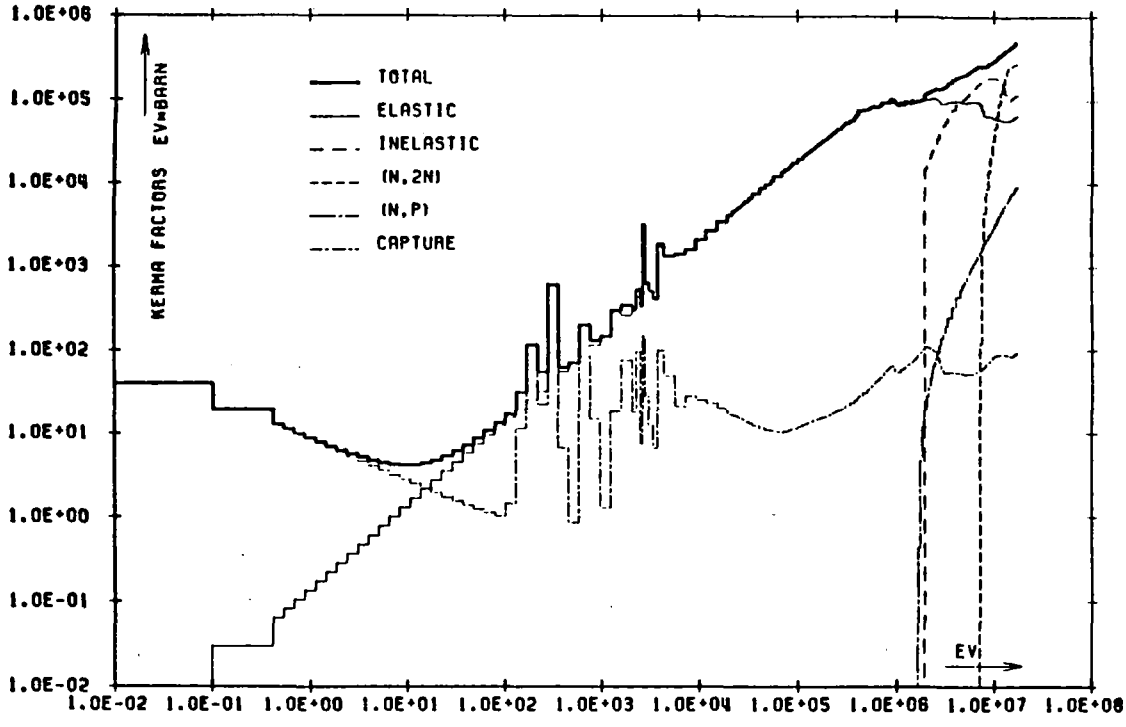

Fig. 2 KERMA factors for Zr+n

References

[1] B. Goel et al., NEANDC(E)-252 U vol. V (1984) p.11

[2] M.T. Swinhoe, private communication (1984)

[3] M.T. Swinhoe and C.A. Uttley,AERE-R-9929 (1980)

[4] A. Takahashi et al., 13th-Symposium on Fusion Technology and private communication

[5] D.L. Smith et al., ANL/NDM-87 (1984)

[6] K. Shibata, JAERI-M 84-204 (1984)

[7] M. Dalle Donne, S. Dorner, S. Taczanowski, KfK 3584 (1983)

[8] Radiation Shielding Information Center, DLC-41 (1979)

[9] Y. Gohar, M.A. Abdou, ANL/FPP/TM-106 (1978)

2. Nuclear Reaction Theory

2.1 Statistical Distributions of S- and R-matrix Elements, Rigorous Calculation of Average Cross Sections

F.H. Fröhner

The problem of resonance-averaged partial cross sections (width fluctuation factors) has been reinvestigated in the context of the statistical model with information-theoretical methods. First results for the case of pure elastic scattering, presented in the last progress report [1], are now generalised to an arbitrary number of reaction channels. The probability distributions of S- and R-matrix elements were found by maximisation of the associated information entropy, subject to the constraint that only the average S-matrix is known, apart from the universal features of the S-matrix, viz.

- unitarity (from overall probability conservation),
- symmetry (from invariance under time reversal),
- no poles in the upper half of the complex energy plane (from causality)

A key step in the derivation is the realisation that with the average S-matrix, $\bar{S}$, one knows also the averages $\overline{S^2} = \bar{S}^2$, $\overline{S^3} = \bar{S}^3$ etc. and thus $\overline{f(S)} = f(\bar{S})$ for any matrix function as matrix functions are defined quite generally as power series. These relationships follow directly from the causality condition if the overbar is understood as an energy average with Lorentzian weight function for easy contour integration. Assuming the Lorentzian to be so wide that many poles (cross section resonances) contribute to the averages we can equate energy averages and ensemble averages. This "analytic ergodicity" [2] entails

$$\langle \ln \det|1-\bar{S}^*S|^2\rangle = \ln \det|1-\bar{S}^*\bar{S}|^2 = 2 \ln \det T, \qquad (1)$$

where $T = 1-\bar{S}^*\bar{S}$ is Satchler's transmission matrix (and 1 the unit matrix). Maximising the information entropy subject to this constraint we find [3], by the method of Lagrange parameters,

$$p(S|\bar{S})d\mu(S) \propto \left(\frac{\det T}{\det|1-\bar{S}^{+}S|^{2}}\right)^{(n+1)/2} d\mu(S) \qquad (2)$$

where n is the number of open reaction channels (the dimensionality of S). The exponent (n+1)/2 results from a second key step: The Lagrange para-parameter corresponding to (1) is determined by the requirement that the marginal distribution of any diagonal R-matrix element R_{cc} be the same Cauchy distribution (Lorentzian) that would pertain if c were the only open channel [1]. Substituting R for S one gets, instead of the less obvious measure $d\mu(S)$, the measure $d\mu(R)$ which is essentially the product of all independent dR_{ab} $(a \leq b)$, and eventually [3]

$$p(R|\bar{R})d\mu(R) = C\left(\frac{\det \pi s}{\det|R-\bar{R}|^{2}}\right)^{(n+1)/2} \prod_{a\leq b} dR_{ab} \ ,$$

$$C = \pi^{-n(n+1)/4} \frac{\Gamma\left(\frac{n+1}{2}\right)}{\Gamma\left(\frac{1}{2}\right)} \prod_{c=1}^{n} \frac{\Gamma(n-c+1)}{\Gamma\left(\frac{n-c}{2}+1\right)} \ , \qquad -\infty<R_{ab}<\infty \ , \qquad (3)$$

where πs is the imaginary part of the "smoothed" R-matrix $\bar{R}$ corresponding to $\bar{S}$. The probability density $p(S|\bar{S})$ is known as the Poisson kernel in the domain of unitary symmetric matrices and has the general property [4]

$$\int d\mu(S)\ p(S|\bar{S})\ f(S) \ = \ f(\bar{S}) \qquad (4)$$

which in our context is nothing but a general statement of analytic ergodicity. The distribution $p(R|\bar{R})$ may be considered as a generalised t-distribution.

Resonance-averaged cross sections can be expressed as expectation values over the distribution $p(S|\bar{S})$. In principle this constitutes a solution to the long-standing Hauser-Feshbach problem. The dimensionality of the resulting integrals is n(n+1)/2 for n open channels. Employing "polar coordinates" (see [4]), i. e. writing $S = O\Lambda O^{T}$, where the orthogonal matrix O represents a pure rotation and Λ is the diagonal matrix with the eigenvalues $\exp(i\vartheta_c)$ as elements, one can reduce the dimensionality to n. For instance, the double integral determining the inelastic cross section for n = 2 and real diagonal $\bar{S}$ is

$$\langle|S_{12}|^{2}\rangle = \frac{\pi}{4} \int_{-\pi}^{\pi} \frac{d\vartheta_1}{2\pi} \int_{-\pi}^{\pi} \frac{d\vartheta_2}{2\pi} \left(\sin^{2}\frac{\vartheta_1-\vartheta_2}{2} \prod_{c=1}^{2} \frac{1-\bar{S}^{2}_{cc}}{1+\bar{S}^{2}_{cc}-2\bar{S}_{cc}\cos\vartheta_c}\right)^{3/2} . \qquad (5)$$

Fig. 3 shows a calculation of the elastic enhancement factor, $\omega = T/\langle|S_{12}|^2\rangle - 1$, for the case of two equivalent channels, compared to the prescriptions due to Moldauer [4] and to Hofmann, Richert, Tepel and Weidenmüller [5], which are heuristic parametrisations of Monte Carlo results obtained from the Statistical Model of resonance reactions. Results of de los Reyes, Mello and Seligman [6] are also shown which correspond to utilisation of first and second powers of $\bar{S}$ only in the maximum entropy algorithm.

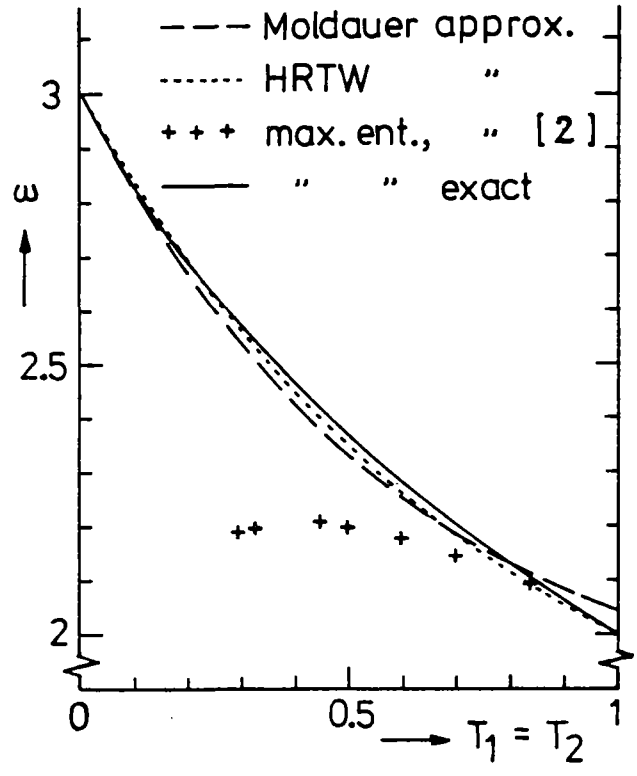

Fig. 3 Elastic enhancement factor for two equivalent channels ($\bar{S}_{11} = \bar{S}_{22} = \sqrt{1 - T_1}$, $\bar{S}_{12} = 0$): rigorous calculation and approximations (see text)

Entropy maximisation leads thus to a solution of the long-standing Hauser-Feshbach problem, permitting the expression of partial cross sections in terms of the average S-matrix. Direct processes are auto-

matically included if S is non-diagonal. There is no restriction to a finite number of eigenstates or to specific ensembles of Hamiltonian matrices such as the Gaussian Orthogonal Ensemble.

References

[1] F.H. Fröhner, NEANDC(E)-252 U, vol. V, p. 16

[2] J. de los Reyes, P.A. Mello and T.H. Seligman, Z. Physik A302 (1981) 351

[3] F.H. Fröhner, Proc. Int. Conf. on Nuclear Data for Basic and Applied Science, Santa Fe, New Mexico, May 13-17, 1985 (in print)

[4] L.K. Hua, Harmonic Analysis of Functions of Several Complex Variables in the Classical Domains (American Math. Soc., Providence, Rhode Island, 1963)

[5] P.A. Moldauer, Nucl. Phys. A344 (1980) 185

[6] H.M. Hofmann, J. Richert, J.W. Tepel and H.A. Weidenmüller, Ann. Phys. 90 (1975) 403

INSTITUT FÜR CHEMIE (1): NUKLEARCHEMIE
KERNFORSCHUNGSANLAGE JÜLICH

1. Neutron Data

1.1 Study of (n,t) Reactions

S.M. Qaim, A. Suhaimi, R. Wölfle

In continuation of our radiochemical studies on fast-neutron induced trinucleon emission reactions [cf. 1] we investigated the effect of spin on the isomer distribution ratios in (n,t) reactions. Cross sections were determined at 14.6±o.4 MeV for the formation of several isomeric pairs [2]. From those data the isomeric cross-section ratios ($\sigma_m/\sigma_m + \sigma_g$) were obtained which are plotted in Fig. 1 as a function of the spin of the isomeric state (J_m). In general the data base is rather weak and any well defined correlation is not discernible. Nonetheless, it appears that in the (n,t) reaction isomeric states are preferentially populated when their spin values lie between 3/2 and 3. This tendency is somewhat different from that observed for the common reactions occurring at 14-15 MeV, viz. (n,p), (n,α) and (n,2n), where the most favoured spin values lie between 4 and 6.

Cross sections were measured for the $^{1o}B(n,t)2\alpha$ process in the energy range of 3 to 8 MeV. B_4C samples were degassed and irradiated with quasi-mono-energetic neutrons using a deuterium gas target at our compact cyclotron [3]. The neutron flux monitoring was done using the $^{58}Ni(n,p)^{58}Co$ and $^{54}Fe(n,p)^{54}Mn$ reactions. The accumulated tritium in the B_4C sample was separated by vacuum extraction and counted in the gas phase using an anti-coincidence system. Several extractions were performed at 12oo°C. The estimated yield of tritium extraction was 95 %; an analysis of the residual gas is in progress to determine the radiochemical yield more accurately. The preliminary cross-section data are shown in Fig. 2 as a function of neutron energy. The values are in general agreement with the scarce data available in the literature. Measurements beyond 8 MeV are underway. In the vicinity of 1o MeV use of highly enriched ^{1o}B is mandatory since the $^{11}B(n,t)^{9}Be$ reaction also starts contributing.

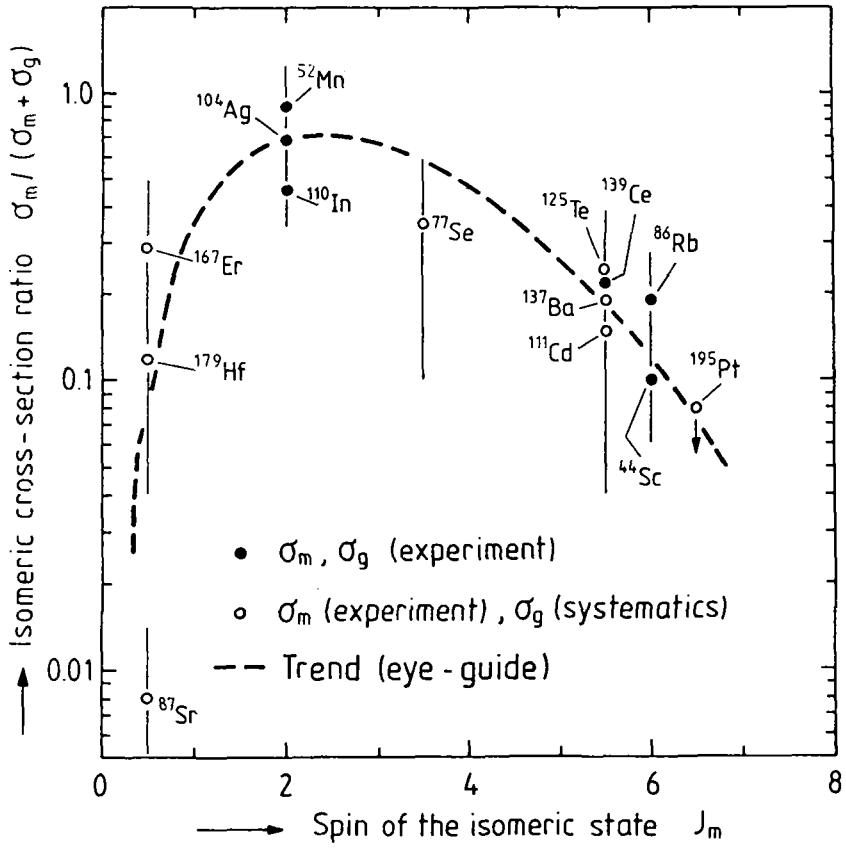

Fig. 1 Isomeric cross-section ratios for (n,t) reaction products at 14.6 ± o.4 MeV as a function of the spin of the isomeric state [2].

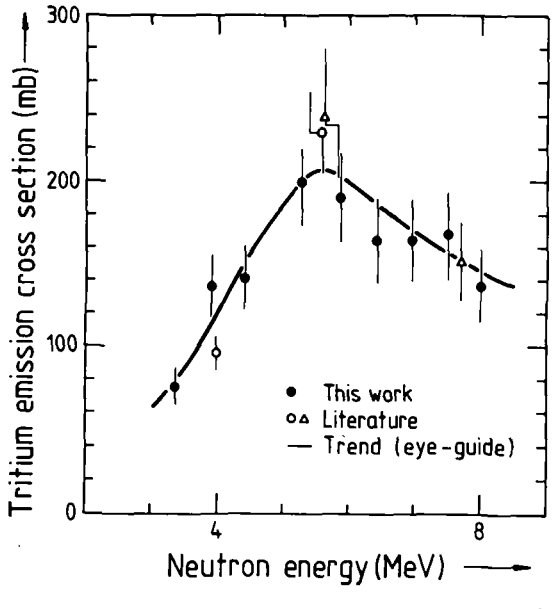

Fig. 2 Triton emission cross sections for the $^{10}B(n,t)2\alpha$ process.

1.2 Helium Emission Cross Sections

S.M. Qaim, M.M. Rahman, R. Wölfle

(Relevant to request identification numbers: 722149F, 724o56F, 732o28F, 732o32F, 732o44R, 76213oF, 762244F, 781o62F, 781o96F, 79211oF, 79221oF, 8o1o64F, 8o1147F)

In continuation of our (n,α) studies [cf. 4] helium production cross sections for elemental nickel were obtained from the activation (n,α) cross sections for ^{58}Ni, ^{62}Ni and ^{64}Ni reported recently [3], and from Hauser-Feshbach calculations or systematics for ^{6o}Ni and ^{61}Ni. At 14.8 MeV the values were raised by 15 % to correct for the (n,n'α) contribution. The results are shown in Fig. 3 together with those obtained by spectral measurements (telescope counter in Geel and quadrupole spectrometer in Livermore) and mass spectrometry (Atomics Int.) as well as those given in data files. Whereas the experimental data are in fair agreement, there is discrepancy between ENDF/B-V and KEDAK values. A new evaluation appears necessary.

The helium production cross sections for elemental molybdenum were obtained from the isotopic activation data [5] and Hauser-Feshbach calculations or systematics, as described above. These results are also shown in Fig. 3 together with the literature values at 14.8 MeV. The data between 6 and 1o MeV have been determined for the first time.

2. Charged Particle Data for Radioisotope Production

Z. Kovács, S.M. Qaim, G. Stöcklin

In continuation of our studies [cf. 6,7] on the production of medically important short-lived radioisotopes, excitation functions of (p,xn) and other competing reactions on 96.5 % enriched ^{76}Se, relevant to the production of ^{75}Br, were measured [8]. The data for the (p,xn) reactions are shown in Fig. 4. The optimum energy range for the production of ^{75}Br at a compact cyclotron is E_p = 24 → 21.5 MeV. In this energy range the literature data lie about 15 % higher than our values. The expected thick target yield of ^{75}Br is 32 mCi/μAh and the level of ^{76}Br-impurity about 2 %.

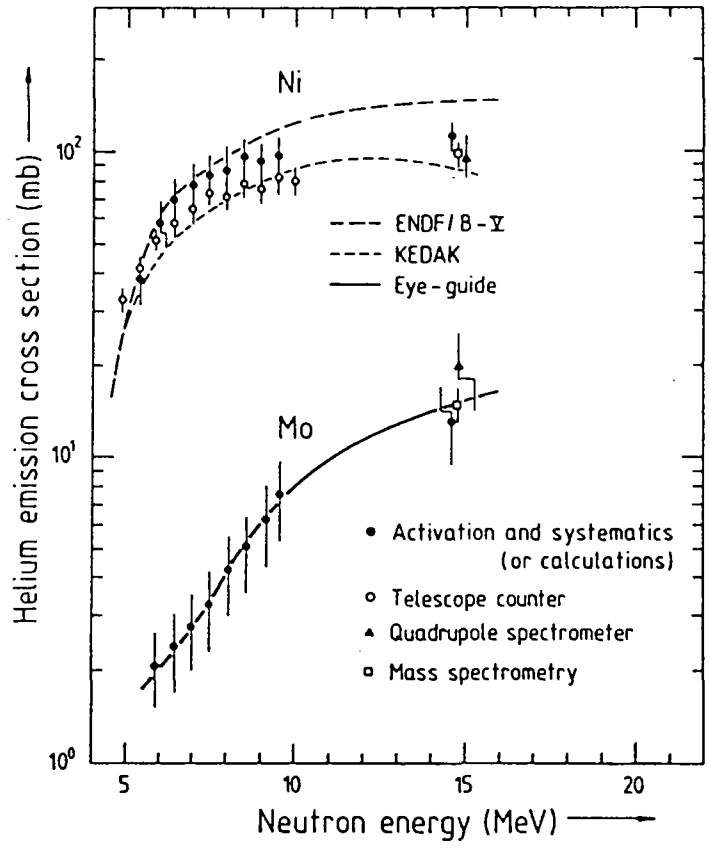

Fig. 3 Helium emission cross sections for elemental nickel and molybdenum.

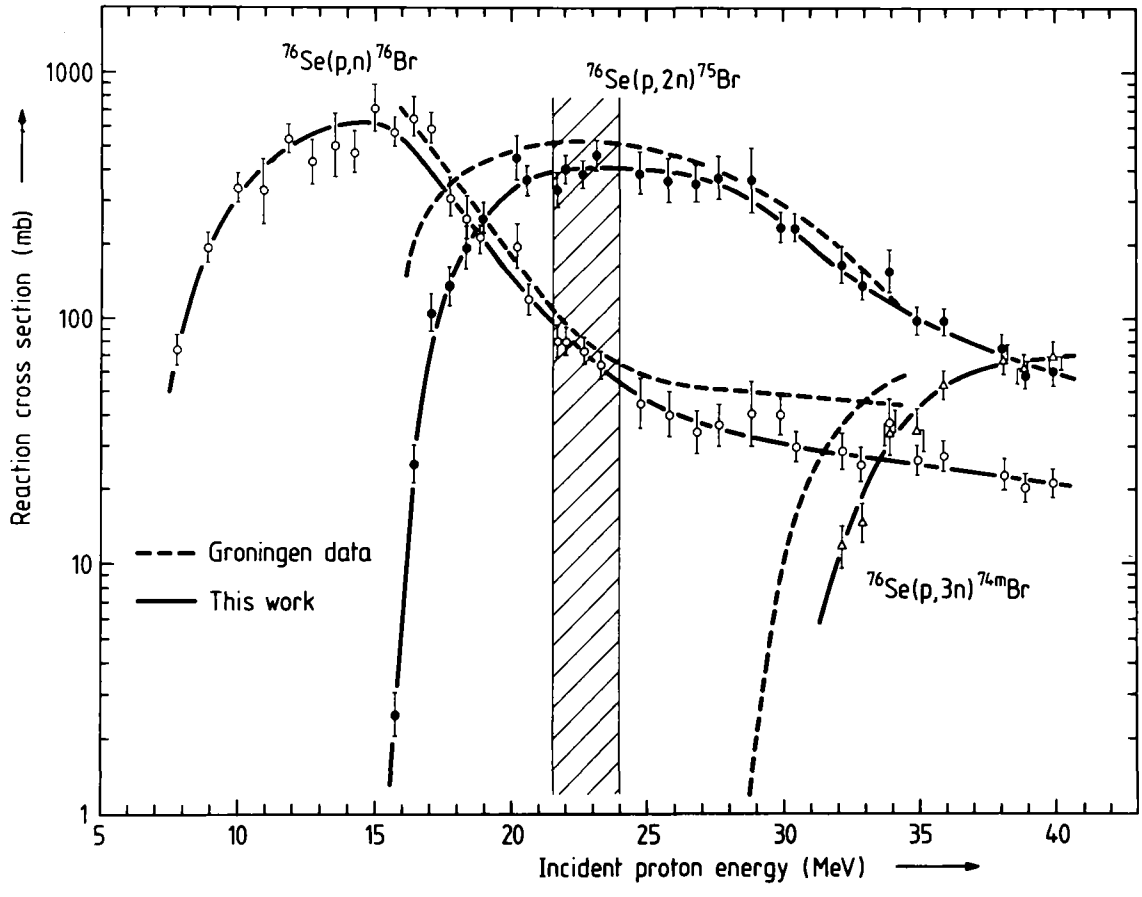

Fig. 4 Excitation functions of (p,xn) reactions on 96.5 % enriched 76- Se

References

[1] R. Wölfle, S. Khatun, S.M. Qaim, Triton emission cross sections with 3o MeV d (Be) break-up neutrons, Nucl.Phys. A423 (1984) 13o

[2] S.M. Qaim, Isomeric cross-section ratios in (n,t) reactions on some medium and heavy mass nuclei at 14.6 MeV, Nucl.Phys. A438 (1985) 384

[3] S.M. Qaim, R. Wölfle, M.M. Rahman, H. Ollig, Measurement of (n,p) and (n,α) reaction cross sections on some isotopes of nickel in the energy region of 5 to 1o MeV using a deuterium gas target at a compact cyclotron, Nucl.Sci. Engineering 88 (1984) 143

[4] S.M. Qaim, Activation cross sections of (n,α) reactions at 14.7 MeV in the region of rare earths, Radiochimica Acta 35 (1985) 35

[5] M.M. Rahman, S.M. Qaim, Excitation functions of some neutron threshold reactions on isotopes of molybdenum, Nucl.Phys. A435 (1985) 43

[6] S.M. Qaim, H.J. Probst, Excitation functions of deuteron induced nuclear reactions on vanadium with special reference to the production of ^{43}K: Systematics of (d,xn) reaction cross sections relevant to the formation of highly neutron deficient radioisotopes, Radiochimica Acta 35 (1984) 11

[7] S.M. Qaim, H. Döhler, Production of carrier-free ^{117m}Sn, Int.J. appl.Radiat.Isotopes 35 (1984) 645

[8] Z. Kovács, G. Blessing, S.M. Qaim, G. Stöcklin, Production of ^{75}Br via the ^{76}Se(p,2n)^{75}Br reaction at a compact cyclotron, in press

INSTITUT FÜR KERNPHYSIK
KERNFORSCHUNGSANLAGE JÜLICH

Fission Yield of a High-Spin Isomer in ^{97}Y

G. Lhersonneau, H. Ohm, K. Sistemich

A new isomer has been discovered [1] in ^{97}Y with the fission product separator JOSEF at the research reactor DIDO of the KFA Jülich. This isomeric level at 3523 keV with a half-life of (144 ± 10) ms is interpreted as a three-quasi-particle state with spin and parity $27/2^-$. The isomeric yield in the fission of ^{235}U is (5.0 ± 1.0) % of the ^{97}Y fission yield [2]. This population can serve as a test for statistical considerations. The feedings into the $1/2^-$ ground state, the $9/2^+$ β-decaying isomer and the new isomer have been calculated adopting the assumption of Ref. [3] for the deexcitation of the prompt γ radiation after fission (see Fig. 1).

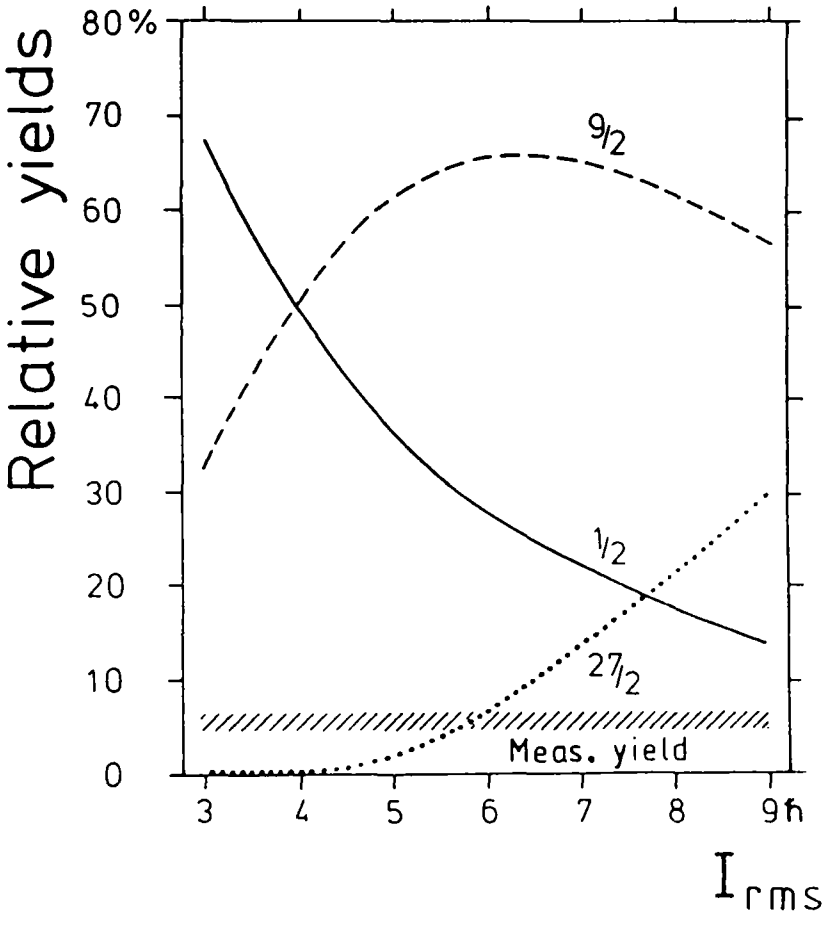

Fig. 1: Calculated fission yields of the $1/2^-$, $9/2^+$ and $(27/2^-)$ levels in ^{97}Y and measured yield of the high-spin isomer.

The result agrees with the experimental value if I rms of the primary spin distribution is taken as 5.9 ± 0.3. This value is in accordance with the one [4,5] which was deduced from the measurements of the isomeric yield ratio for the $9/2^+$ and $1/2^-$ levels, and it demonstrates the validity of the statistical approach also for high-spin states.

[1] G. Lhersonneau, D. Weiler, P. Kohl, H. Ohm, K. Sistemich: Ann. Rept. 1984, IKP, Kernforschungsanlage Jülich, in press

[2] H. Wollnick, G. Siegert, J. Greif, G. Fiedler, Proc. 3rd Int. Conf. on Nuclei far from Stability, Cargese, France 1976, Report CERN 76-13, p. 517

[3] D.G. Madland, T.R. England: Nucl. Sci. Engineering 64 (1977) 859

[4] J.P. Bocquet, F. Schussler, E. Monnand, K. Sistemich: Proc. of the 4th IAEA Symposium on the Physics and Chemistry of Fission, Jülich, F.R. Germany 1979, IAEA Vienna, 1980, Vol. II, p. 179

[5] St. Hörner, H.O. Denschlag, W. Ditz, U. Güttler, B. Sohnius, P. Stumpf, H. Faust, Verhandl. DPG (VI) 20 (1985) 530

INSTITUT FÜR REINE UND ANGEWANDTE KERNPHYSIK
UNIVERSITÄT KIEL, GKSS-FORSCHUNGSZENTRUM GEESTHACHT

Fast-Chopper Neutron Time-of-Flight Spectrometer*

H.G.Priesmeyer, B.Asmussen, U.Harz, P.Henkens, P.Fischer

1. Transmission and Resolution of a Chopper System for Epithermal Neutrons

The results of a MONTE-CARLO calculation for the realistic case of the Kiel Fast-Chopper time-of-flight spectrometer have been verified by experimental investigations. Therefore the geometry and the material composition of the system as well as diverging neutron paths have been considered. The assumption of a Gaussian-shaped resolution function is shown to be justified, but its width for a "grey" rotor-collimator system is 15% larger than that for a "black" system. The physical consequence of this result is a systematic overestimation of the parameters determined by SHAPE analysis. Direct measurement of the resolution function of a chopper system would imply the availability of an extremely monoenergetic neutron source. But the numerical results describe other features that give better access to experimental verification so well, that we conclude to have calculated a better resolution function now (cf. also Fig.1).
The programs are in a form which can be adopted to problems for calculating choppers as mechanical pulse shorteners at an intense neutron source like SNQ.

2. Resonance Parameters of the 5.4 eV Level in Dy-162

The experiments on dysprosium (request 82047 DOE/NDC 28 U) have been concluded by a measurement of the transmission around 5.4 eV on a sample of 92.39% enriched dysprosiumoxide (0.9 g), diluted in heavy water.
The preliminary parameters determined by SHAPE analysis are :

$$E_0 = 5.458 \text{ eV}$$
$$\Gamma = 119.9 \text{ meV}$$
$$\Gamma_n = 30.4 \text{ meV}$$

3. Low-energy Low-temperature Transmission of Aluminum Alloy

The alloy AlMg3 (Werkst.Nr.3.3535.20 DIN 1790) will be the structural material for the moderator vessel of the future cold neutron source at the Geesthacht reactor. The form of this moderator vessel will be lens-shaped, 6 cm thick,with a wall thickness of 6 mm in order to withstand the pressure of its supercritical hydrogen filling. Therefore the transmission of the wall for cold neutrons is of importance to the gain. The total

*Work supported by GKSS under contract 291897

cross section has been measured in the low energy range, considering the fact that below the BRAGG edge at about 5 meV it is strongly temperature dependent.
The experiment shall be extended to 4 K.

4. Iron-filter Difference Transmission with Good Energy Resolution

In cooperation with the CBNM in Geel/Belgium the transmission of the Kiel combined iron-filter has been measured at 98 m and up to 1 MeV at Gelina. This was important, since the filter difference shall be used for cross section work especially on the Kiel radioactive samples and corrections for systematic errors due to high-energy contamination have to be studied. This contamination has been shown to be less than 1% of the window line at 24 keV.
To proove the adequacy of the instrument, a precise determination of the n,p total cross section has been made, the preliminary result being in agreement with the shape-independent effective-range approximation using the Lomon/Wilson parameters. Figure 2 shows the filter difference transmission at 24 keV as determined by the linac measurement.
The kind support by Dr. Brusegan of CBNM, who has made the transmission measurement, shall be gratefully acknowledged.

5. Publications

P.Henkens, P.Fischer, U.Harz, H.G.Priesmeyer
24.4 keV Neutron Beam Filter Facility at FRG-I
ATKE 46 (1985) 50

H.G.Priesmeyer
Sequentielle Analyse der Daten eines Monitors für radioaktive Strahlung
GKSS 84/E/3

P.Henkens
Bau und Test eines optimierten Eisenfilters für 24,4 keV Neutronen
GKSS 84/E/30

B.Asmussen, P.Fischer, U.Harz, H.G.Priesmeyer
Auflösung und Transmission eines Fast-Chopper Flugzeitspektrometers
Innsbruck 1984, DPG-Verhandlungen S. 1037

P.Fischer, U.Harz, H.G.Priesmeyer
Die Resonanzparameter des Dysprosium-162 bei 5,4 eV
Innsbruck 1984, DPG-Verhandlungen S. 923

H.G.Priesmeyer
Recent work at the Kiel University Fast-Chopper
European Interlab Seminar , Braunschweig, 1984

P.Henkens, P.Fischer, U.Harz, H.G.Priesmeyer
24.4 keV Neutron Beam Facility at the Reactor FRG-I
European Interlab Seminar, Braunschweig, 1984

B.Asmussen, P.Fischer, U.Harz, H.G.Priesmeyer
Resolution and Transmission of a Fast-Chopper TOF Spectrometer

H.G.Priesmeyer
A Novel Random-Pulser Concept for Empirical Reliability Studies
GKSS 85/E/5

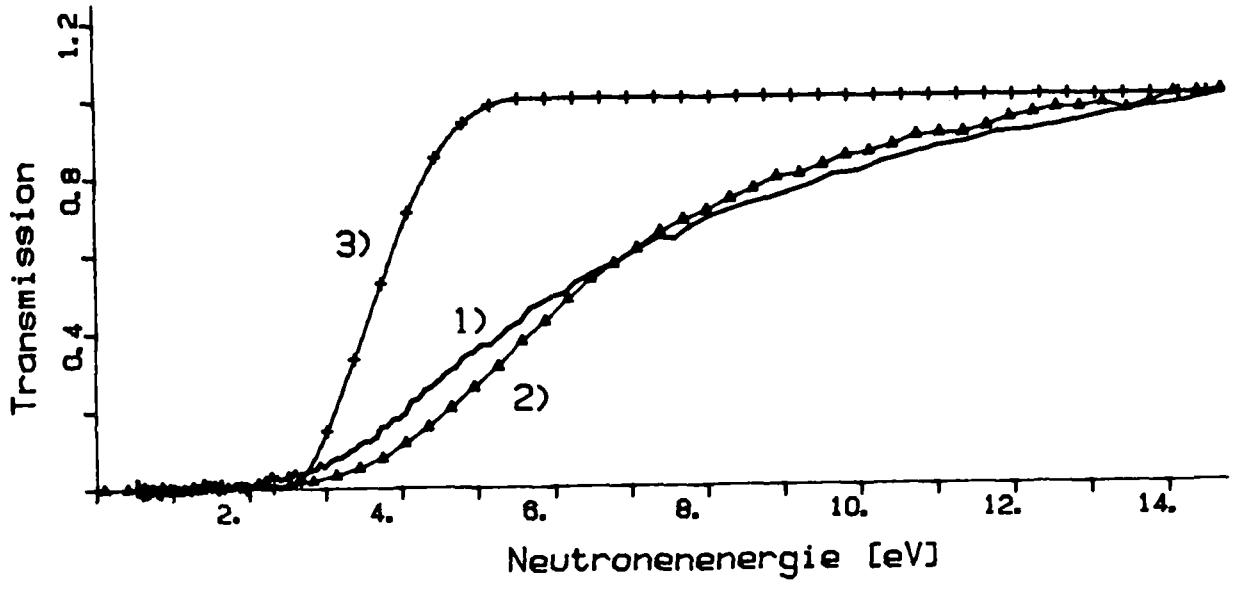

Fig.1 Chopper cut-off function for 5000 rpm

1) experimental result
2) Monte-Carlo result for "grey" chopper system
3) Monte-Carlo result for "black" chopper system

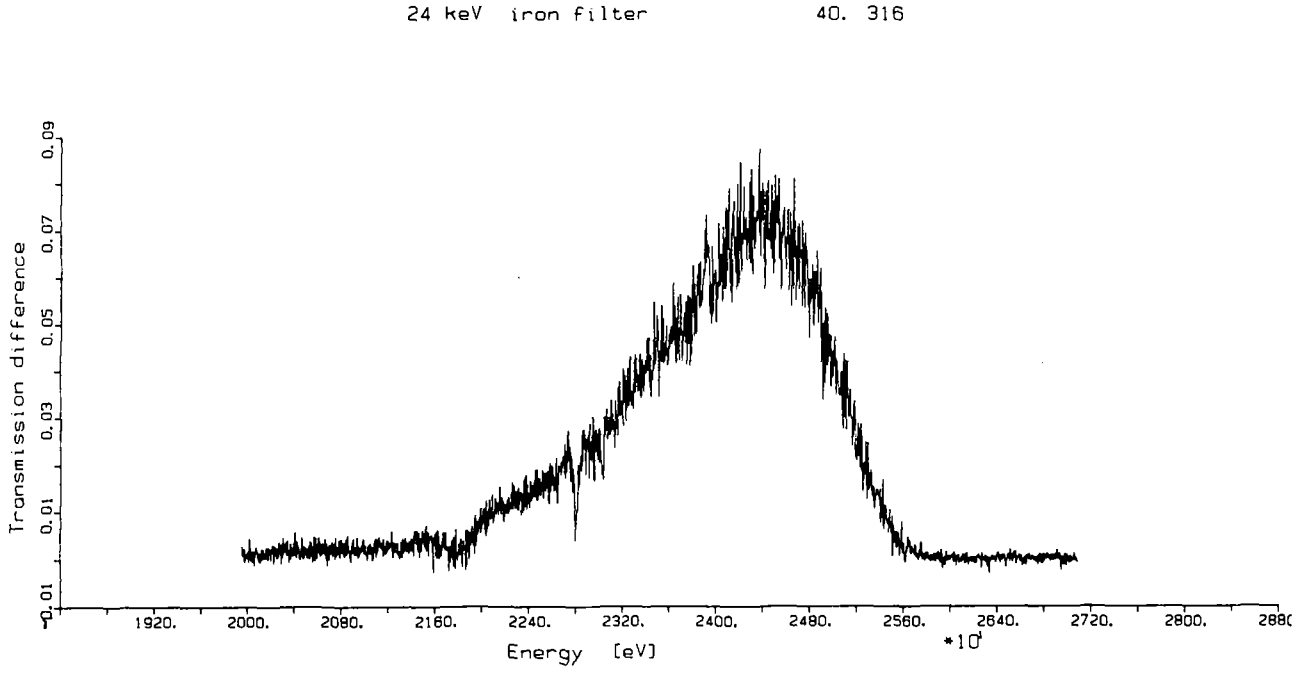

Fig.2 Iron-titanium filter difference transmission at 24 keV neutron energy

INSTITUT FÜR PHYSIK
GKSS-FORSCHUNGSZENTRUM GEESTHACHT

14 MeV Neutron Activation Cross Sections

R. Pepelnik, B. Anders, B.M. Bahal, M. Farooq

The high intense neutron generator facility KORONA [1] is mainly used for activation analysis. Exact knowledge of the concerning cross sections is prerequisite to this work. The cylindrical target structure of KORONA leads to a neutron energy distribution with a median at 14.7 MeV and a FWHM of 0.6 MeV [2]. The reaction cross sections used in activation analysis must fit accurately to the applied neutron spectrum. Utilizing cross sections measured at KORONA, the analysis errors are reduced, because the uncertainties of literature values, due to the energy-dependence of cross sections and to nuclear decay data, are cancelled.

Samples from material of high purity containing Na, Mg, Al, Si, P, Cl, K, Ca, Sc, Ti, V, Cr, Cu, Rb, Sr, Zr, Nb, Mo, In, Sb, I, Ba, Pb and U were investigated as targets for neutron activation. For analysis of Ti, Zn, Mo, Cd and Ba isotopically enriched samples of ^{46}Ti, ^{50}Ti, ^{68}Zn, ^{70}Zn, ^{92}Mo, ^{97}Mo, ^{110}Cd, ^{111}Cd, ^{114}Cd, ^{116}Cd, ^{136}Ba, ^{137}Ba and ^{138}Ba were available.

The neutron flux monitoring was done via the well known reactions ^{93}Nb(n,2n) and ^{27}Al(n,α). According to the half-lives of the radio-isotopes to be analyzed Mg or Al or Rb or Nb was added to and homogeneously mixed with the samples to get an optimum adapted neutron flux monitor [3].

The reaction cross sections determined by cyclic or conventional activation technique are summarized in Table I. More details about the measurements as well as a comparison with literature values are given in Refs. [3] and [4].

Table I Activation Cross Sections at 14.7 ± 0.3 MeV

Reaction	σ (mb)	Ref.
$^{23}Na(n,p)^{23}Ne$	47 ± 2	[4]
$^{23}Na(n,\alpha)^{20}F$	123 ± 4	[4]
$^{25}Mg(n,p)^{25}Na$	63 ± 4	[4]
$^{26}Mg(n,p)^{26}Na$	20 ± 4	[4]
$^{26}Mg(n,\alpha)^{23}Ne$	52.0 ± 1.3	[3]
$^{27}Al(n,p)^{27}Mg$	69.0 ± 1.7	[3]
$^{27}Al(n,\alpha)^{24}Na$	114 ± 3	[3]
$^{28}Si(n,p)^{28}Al$	265 ± 11	[4]
$^{29}Si(n,p)^{29}Al$	138 ± 6	[4]
$^{31}P(n,{}^{3}He)^{29}Al$	0.03 ± 0.01	[4]
$^{35}Cl(n,2n)^{34m}Cl$	7.2 ± 0.3	[4]
$^{39}K(n,2n)^{38}K^{*}$	3.6 ± 0.2	[3]
$^{41}K(n,p)^{41}Ar$	50.7 ± 1.3	[3]
$^{41}K(n,\alpha)^{38}Cl$	33.0 ± 1.3	[3]
$^{42}Ca(n,p)^{42}K$	187.0 ± 8.2	[3]
$^{43}Ca(n,p)^{43}K$, $^{44}Ca(n,np)^{43}K$	150.0^{+} ± 8.2	[3]
$^{44}Ca(n,p)^{44}K$	44.0 ± 7.5	[3]
$^{44}Ca(n,\alpha)^{41}Ar$	29.0 ± 1.2	[3]
$^{48}Ca(n,2n)^{47}Ca$	850 ± 35	[3]
$^{45}Sc(n,\alpha)^{42}K$	56.0 ± 2.3	[3]
$^{45}Sc(n,2n)^{44m}Sc$	130.4 ± 4.9	[3]
$^{46}Ti(n,p)^{46m}Sc$	62.6 ± 3.0	[3]
$^{46}Ti(n,p)^{46}Sc^{*}$, $^{47}Ti(n,d)^{46}Sc^{*}$	304^{+} ± 10	[4]
$^{47}Ti(n,p)^{47}Sc$, $^{48}Ti(n,d)^{47}Sc$	257^{+} ± 12	[4]
$^{48}Ti(n,p)^{48}Sc$, $^{49}Ti(n,d)^{48}Sc$	68.7^{+} ± 2.1	[4]
$^{50}Ti(n,p)^{50m}Sc$	8.7 ± 0.5	[3]
$^{50}Ti(n,p)^{50}Sc^{*}$	14.1 ± 1.3	[3]
$^{50}Ti(n,\alpha)^{47}Ca$	8.5 ± 0.5	[4]
$^{51}V(n,p)^{51}Ti$	28.8 ± 1.5	[4]
$^{51}V(n,\alpha)^{48}Sc$	15.0 ± 1.0	[3]
$^{51}V(n,n'\alpha)^{47}Sc$	0.07 ± 0.01	[3]
$^{50}Cr(n,2n)^{49}Cr$	25.0 ± 1.0	[3]
$^{52}Cr(n,p)^{52}V$, $^{53}Cr(n,np)^{52}V$	87.0^{+} ± 2.3	[3]
$^{53}Cr(n,p)^{53}V$	46.0 ± 1.5	[3]
$^{65}Cu(n,p)^{65}Ni$	20 ± 1	[4]
$^{68}Zn(n,p)^{68m}Cu$	6.1 ± 0.4	[3]
$^{68}Zn(n,p)^{68}Cu$	9.1 ± 0.7	[3]
$^{70}Zn(n,p)^{70m}Cu$	4.1 ± 0.3	[3]
$^{70}Zn(n,p)^{70}Cu$	2.9 ± 0.3	[3]
$^{85}Rb(n,p)^{85m}Kr$	4.6 ± 0.2	[4]
$^{85}Rb(n,\alpha)^{82}Br$	6.9 ± 0.2	[4]
$^{85}Rb(n,2n)^{84m}Rb$	474 ± 14	[4]
$^{85}Rb(n,2n)^{84}Rb^{*}$	1144 ± 35	[4]
$^{87}Rb(n,p)^{87}Kr$	11.6 ± 0.5	[4]
$^{87}Rb(n,2n)^{86m}Rb$	559 ± 17	[3]
$^{87}Rb(n,2n)^{86}Rb^{*}$	1352 ± 42	[4]
$^{86}Sr(n,2n)^{85m}Sr$, $^{84}Sr(n,\gamma)^{85m}Sr$	225^{+} ± 7	[4]
$^{88}Sr(n,\alpha)^{85m}Kr$	1.52 ± 0.09	[4]
$^{88}Sr(n,2n)^{87m}Sr$, $^{86}Sr(n,\gamma)^{87m}Sr$	268^{+} ± 8	[4]
$^{90}Zr(n,p)^{90m}Y$, $^{91}Zr(n,np)^{90m}Y$	12.4^{+} ± 0.8	[3]
$^{90}Zr(n,\alpha)^{87m}Sr$	3.9 ± 0.2	[3]
$^{90}Zr(n,2n)^{89}Zr^{*}$	754 ± 29	[3]
$^{91}Zr(n,p)^{91m}Y$	18.5 ± 0.7	[3]
$^{92}Zr(n,p)^{92}Y$	19.2 ± 1.8	[3]
$^{94}Zr(n,p)^{94}Y$	9.6 ± 0.6	[3]
$^{94}Zr(n,\alpha)^{91}Sr$	4.3 ± 0.4	[3]
$^{96}Zr(n,2n)^{95}Zr$	1420 ± 81	[3]
$^{96}Zr(n,\gamma)^{97}Zr$	0.12 ± 0.01	[4]

Table I cont.

Reaction	σ (mb)	Ref.	Reaction	σ (mb)	Ref.
$^{93}Nb(n,\alpha)^{90m}Y$	5.20 ± 0.33	[3]	$^{127}I(n,2n)^{126}I$	1655 ± 173	[3]
$^{93}Nb(n,n'\alpha)^{89m}Y$	2.10 ± 0.13	[3]	$^{132}Ba(n,2n)^{131m}Ba$	489 ± 30	[4]
$^{93}Nb(n,2n)^{92m}Nb$	462 ± 12	[3]	$^{134}Ba(n,2n)^{133m}Ba$	788 ± 41	[4]
$^{92}Mo(n,p)^{92m}Nb$	72 ± 4	[4]	$^{136}Ba(n,p)^{136}Cs^{*}$	7.75 ± 0.38	[4]
$^{92}Mo(n,\alpha)^{89}Zr^{*}$	26 ± 2	[4]	$^{136}Ba(n,2n)^{135m}Ba$	1180 ± 79	[4]
$^{92}Mo(n,2n)^{91}Mo^{*}$	190 ± 10	[4]	$^{136}Ba(n,n')^{136m}Ba$	46.0 ± 2.3	[3]
$^{96}Mo(n,p)^{96}Nb$	19 ± 1	[4]	$^{137}Ba(n,n')^{137m}Ba$	214 ± 15	[3]
$^{97}Mo(n,p)^{97}Nb^{*}$	18.8 ± 0.9	[4]	$^{138}Ba(n,p)^{138m}Cs$	1.3 ± 0.2	[3]
$^{98}Mo(n,p)^{98m}Nb$	4.0 ± 0.2	[4]	$^{138}Ba(n,p)^{138}Cs$	2.1 ± 0.2	[3]
$^{110}Cd(n,p)^{110}Ag$	21 ± 1	[3]	$^{138}Ba(n,\alpha)^{135m}Xe$	0.75 ± 0.07	[3]
$^{111}Cd(n,p)^{111m}Ag$	47.7 ± 7.2	[3]	$^{138}Ba(n,\alpha)^{135}Xe^{*}$	2.51 ± 0.11	[4]
$^{111}Cd(n,n')^{111m}Cd$	134 ± 10	[3]	$^{138}Ba(n,2n)^{137m}Ba$	1009 ± 50	[3]
$^{114}Cd(n,p)^{114}Ag$	12.0 ± 0.9	[3]	$^{138}Ba(n,2n)^{137m}Ba$ / $^{137}Ba(n,n')^{137m}Ba$	1043^{+} ± 73	[3]
$^{116}Cd(n,p)^{116m}Ag$	0.92 ± 0.11	[3]	$^{138}Ba(n,\gamma)^{139}Ba$	3.3 ± 0.6	[4]
$^{116}Cd(n,p)^{116}Ag^{*}$	2.5 ± 0.3	[3]	$^{204}Pb(n,2n)^{203m1}Pb$	1110 ± 60	[4]
$^{115}In(n,\alpha)^{112}Ag$	2.4 ± 0.2	[4]	$^{204}Pb(n,2n)^{203}Pb^{*}$	1860 ± 90	[4]
$^{115}In(n,n')^{115m}In$	90.5 ± 4.5	[4]	$^{238}U(n,2n)^{237}U$	633 ± 44	[3]
$^{121}Sb(n,2n)^{120m}Sb$	546 ± 20	[4]			

*The value refers to the sum of groundstate and isomeric state cross sections.

+The value is calculated taking the abundance of the first mentioned isotope.

References

[1] H.-U. Fanger, R. Pepelnik, W. Michaelis;
J. Radioanal. Chem. 61 (1981) 147, GKSS-report 81/E/30.

[2] B.M. Bahal, H.-U. Fanger;
Nucl. Instr. and Meth. 220 (1984) 517,GKSS-report 84/E/14.

[3] B. Anders, B.M. Bahal, R. Pepelnik;
GKSS-report 85/E/ to be published.

[4] B.M. Bahal, E. Bössow, M. Farooq, R. Pepelnik;
GKSS-report 85/E/ to be published.

INSTITUT FÜR KERNCHEMIE
UNIVERSITÄT ZU KÖLN

1. Thick Target and Thin Target Production Data Relevant to the Interpretation of the Interaction of Galactic Protons with Extra-terrestrial Matter

R. Michel[+], P. Dragovitsch, F. Peiffer, S. Theis

1.1 Production of Spallogenic Nuclides in Spherical Diorite Targets Homogeneously Irradiated with 600 MeV Protons

In order to simulate the interaction of galatic protons with small stony meteorites three thick target irradiation experiments have been performed at the 600 MeV p-beam of the CERN synchro cyclotron. In these experiments combined thin target / thick target arrangements were irradiated. The thick targets were spheres with a radii of 5, 15, 25 cm made out of diorite which due to its chemical composition, high density and low water content is well suitable to simulate stony meteorites. These spheres contained a wide variety of pure element foils, selected chemical compounds and degassed meteoritic material. Figure 1 gives a survey of the target arrangement used in the first irradiation. By complex movements of the artificial meteorites during irradiation a homogeneous 4 π irradiation was achieved. Depth profiles for the production of spallogenic radionuclides as well as of stable rare gas isotopes were measured using gamma-spectroscopy, conventional and accelerator mass spectroscopy and low level counting techniques. The results demonstrate [1-4] that also in small meteorites the action of secondary particles can by no-means be neglected, and that in contrast to former assumptions also in small objects variations of the production of spallation products with depth have to be accounted for. A survey on the production of radionuclides from iron in an artificial meteorite of 10 cm diameter is given in Fig. 2.

[+] Now at Zentraleinrichtung fuer Strahlenschutz, Univ. Hannover

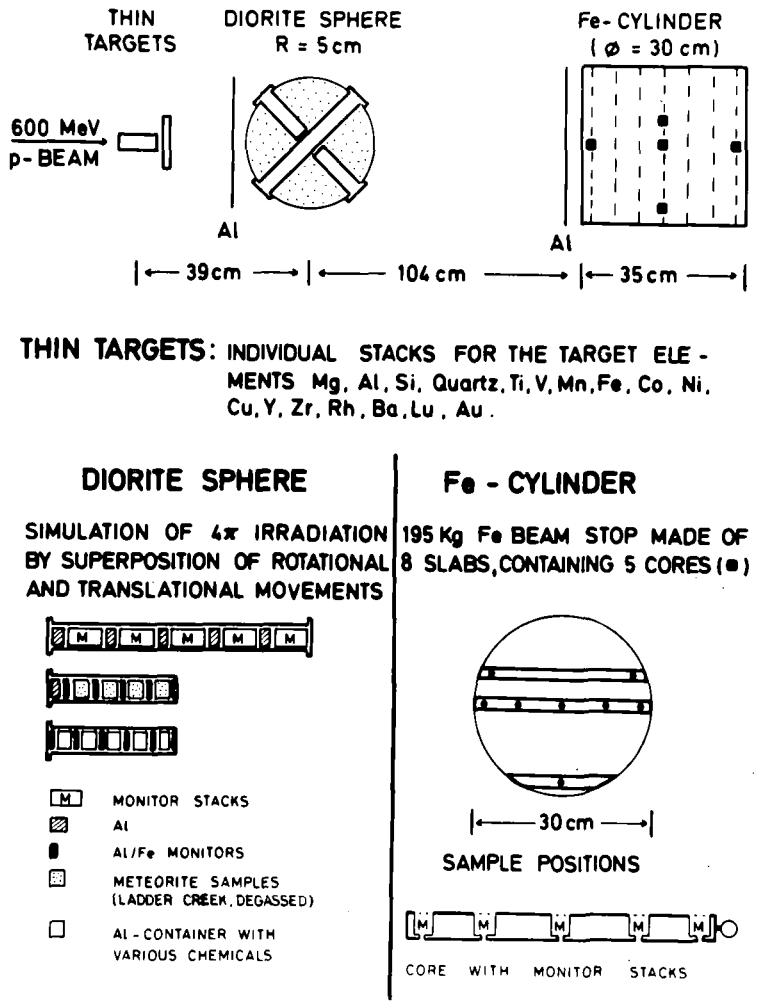

Fig. 1 Target arrangement used in the first irradiation of experiment CERN SC96.

1.2 Evaluation of Excitation Functions for p-induced Reactions up to 10 GeV

In order to combine thin target and thick target approaches for the interpretation of the interaction of galactic cosmic rays with meteorites a compilation and evaluation of thin target cross sections for the production of radionuclides and of stable rare gas isotopes from target elements as O, Mg, Al, Si, Ti, V, Mn, Fe, Co, Ni, Cu, Ba, Lu,

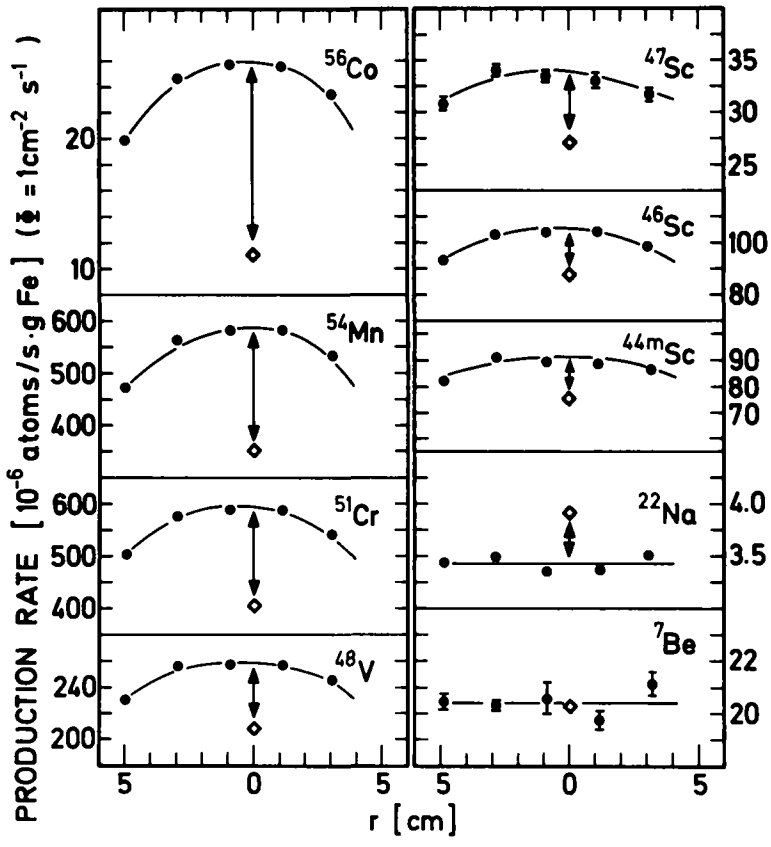

Fig. 2 Production of radionuclides from iron in an artificial meteorite with 10 cm diameter. "◇" gives the production rate in the center due to primary protons only, assuming σ(565 MeV) = σ(600 MeV). The arrows indicate the production by secondary nucleons.

and Au up to p-energies of 10 GeV was initiated. For the target elements Ti, V, Mn, Fe, Co and Ni our recent measurements up to 200 MeV [5,6] together with our thin target measurements at 600 MeV now represent a consistent set of data for the formation of a wide variety of radionuclides. On the basis of this data set it is possible in many cases to decide unambiguously about the quality of earlier partially highly discrepant measurements. In Fig. 3,

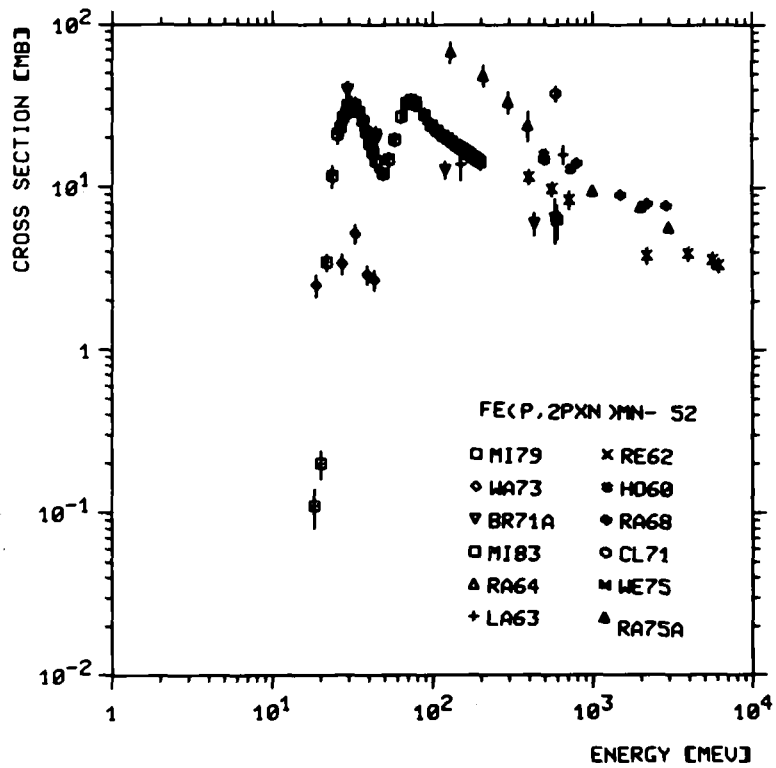

Fig. 3 Cross section data for the production of ^{52}Mn from Fe. For detailed references see [5].

this is shown as an example for the production of ^{52}Mn from Fe. Presently, for the other target elements the status of knowledge is being evaluated and a survey on further necessary experiments is prepared. Furthermore, a comparison with theoretical [7] and semi-emperically calculated [8,9] excitation functions is done in order to estimate the reliability and applicability of these calculational methods for the various fields of applications of medium and high energy reactions.

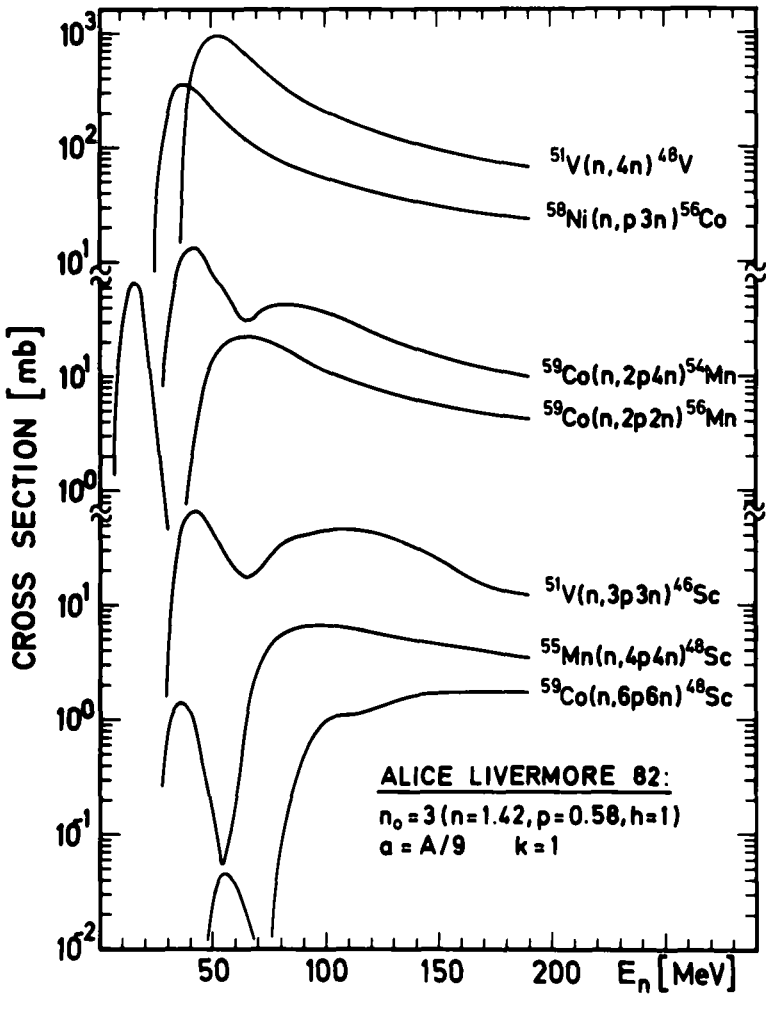

Fig. 4 Excitation functions of n-induced reactions calculated according to [7].

1.3 Theoretical Estimates of Cross Sections for Radionuclide Formation by High Energy Neutrons

For the understanding of the cosmic ray interactions with extraterrestrial matter as well as for the recent developments of spallation neutron sources the knowledge of cross section data for high energy neutron induced reactions is essential. Since there are no experimental thin target data available for energies above 30 MeV an attempt

was made to predict integral excitation functions for the production of radionuclides from Mg, Al, Si, Ti, V, Cr, Mn, Fe, Co, Ni, Cu, Te, Lu, W, and Au for n-energies from 2 to 190 MeV on the basis of the hybrid model [10] in the form of the computer code ALICE LIVERMORE 82 [7]. The theoretical data are compiled [11] and presently tested as far as low energy experimental data are available. On the basis of this comparison and the experiences with hybrid model calculations for p-induced reactions, a critical evaluation is being done. The n-cross sections are used to reproduce the contribution of secondary neutrons to the production of spallogenic nuclides in the above mentioned artificial meteorites using nucleon fluxes derived from Monte-Carlo calculations.

References

[1] R. Michel et al., Lun. Planet. Sci. XV (1984) 542

[2] R. Michel et al., LPI Techn. Rep. (1984), in press

[3] P. Englert et al., Nucl. Instr. Methods Phys. Res. B5 (1984) 415

[4] R. Michel et al., to be submitted to Nucl. Instr. Methods Phys. Res. (1985)

[5] R. Michel et al., Proc. 14th Lun. Planet. Sci. Conf., J. Geophys. Res. 89 (1984) B 673

[6] R. Michel et al., submitted to Nucl. Phys. A (1985)

[7] M. Blann et al., UCID-19614 (1982)

[8] G. Rudstam, Z. Naturforsch. 21A (1966) 1027

[9] R. Silberberg et al., Astrophys. J. Suppl. 220 (1973) 315 and 335

[10] M. Blann, Phys. Rev. Lett. 27 (1971) 337

[11] F. Peiffer et al., KC-NSIG84 (1984), unpublished

INSTITUT FÜR KERNCHEMIE

UNIVERSITÄT MAINZ

1. Fission Yields and Isomeric Ratios

1.1 Isomer Ratios of ^{96}Y, ^{97}Y, and ^{98}Y in the Fission of Uranium-235 with Thermal Neutrons

H.O. Denschlag, W. Ditz, H. Faust*, U. Güttler, ST. Hörner, B. Sohnius, P. Stumpf

The independent yields of the isomers of ^{96}Y, ^{97}Y, and ^{98}Y at various kinetic energies of the fission fragments were determined at the mass separator LOHENGRIN of the Institut Laue-Langevin (Grenoble). The beam of mass separated fission fragments was caught in a moving tape and transported continuously to a shielded Ge(Li)-detector (tape speeds: A=96: 100; A=97: 400; A=98: 250 mm/s). The γ-ray spectra recorded were used to calculate the fractional independent yields of the high- and low-spin isomers of ^{97}Y ($[9/2^+]/[1/2^+]$) and ^{98}Y ($[4^+]/[1^+]$) and of the high-spin isomer of ^{96}Y ($[3^+]^?$). The evaluation of the γ-ray spectra is based on published decay characteristics (A=96 [1], A=97 [2], and A=98 [3]). The low-spin isomer of ^{96}Y ($[0^+]$) does not emit γ-rays and has been obtained from the difference of both isomers [4] minus high spin-isomer. Direct measurements of this isomer using conversion electrons are in preparation.

The fractions of high-spin isomer relative to the (independent) yield of both isomers are shown in Fig. 1 as a function of the kinetic energy of the fission fragments. The results at the mean kinetic energy (∿100 MeV) may be compared with predictions for radiochemical values of F_H=0.90 for ^{96}Y and F_H=0.81 for ^{97}Y and ^{98}Y, respectively. Within the uncertainties of experiment and mo-

*Institut Laue-Langevin, Grenoble, France

del F_H (^{97}Y) agrees well with the prediction. The results of ^{96}Y and, even more, of ^{98}Y deviate, however, strongly from the predicted values.

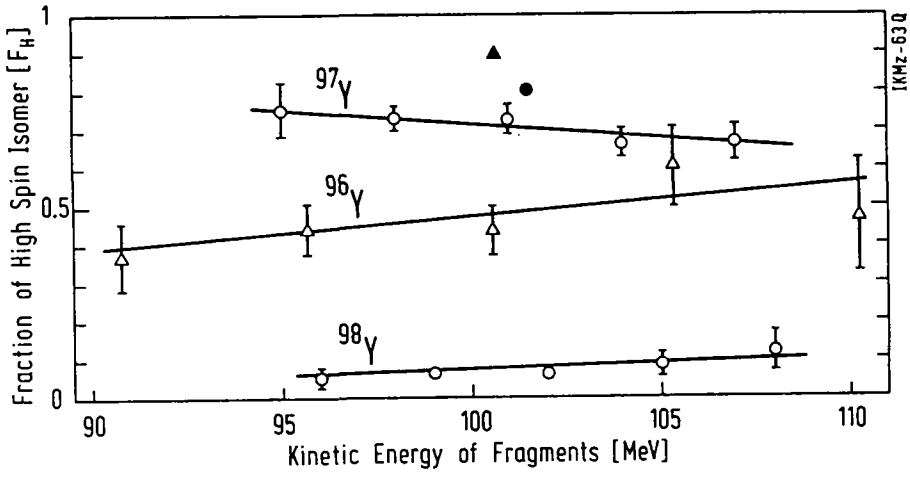

Fig. 1 Fraction of the high-spin isomers of ^{96}Y, ^{97}Y, and ^{98}Y at various (initial) kinetic energies of the fission fragments (at the mean ionic charge state $q=21^+$). (Open symbols: experimental values; closed circle: prediction for ^{97}Y and ^{98}Y, closed triangle: prediction for ^{96}Y)

Similar discrepancies have been noted earlier for ^{99}Nb: $F_H<0.2$ [6] and recently for ^{148}Pr: $F_H=0.12\pm0.03$ [7]. In the two latter cases the prediction amounts also to $F_H=0.81$ [5]. Low experimental values of some indium isotopes with even mass numbers will be referred to in the following contribution.

A decrease of F_H for ^{97}Y with increasing kinetic energy of the fragments is shown in Fig. 1. This observation is in agreement with earlier observations [8] that have been interpreted to indicate a less important transfer of angular momentum in a compact scission configuration of two nearly spherical fragments. Again ^{96}Y and ^{98}Y show different results.

References

[1] H.W. Müller, Nucl. Data Sheets 35 (1982) 281
[2] C.M. Lederer, V.S. Shirley (Eds.) Table of Isotopes, 7th Ed., Wiley (1978)
[3] H.W. Müller, Nucl. Data Sheets 39 (1983) 467
[4] W. Lang et al., Nucl. Phys. A345 (1980) 34
[5] D.G. Madland, T.R. England, Nucl. Sci. and Eng. 64 (1977) 859
[6] M. Weis, H.O. Denschlag, J. Inorg. Nucl. Chem. 43 (1981) 437
[7] C. Chung, L.-J. Yuan, W. B. Walters, Z. Phys. A, Atoms and Nuclei 319 (1984) 295
[8] H.O. Denschlag et al., in Physics and Chemistry of Fission (Proc. Symp. Jülich) IAEA, Vienna (1980), Vol. II, p. 153

1.2 Yields and Isomer Ratios of $^{123-129}$In in the Fission of Uranium-235 with Thermal Neutrons

St. Hörner, H.O. Denschlag, H. Gabelmann, K.L. Kratz, B. Pfeiffer*, U. Stöhlker*

The cumulative yields and the isomeric ratios of $^{123-129}$In were determined using the mass separator OSTIS (ILL, Grenoble) equipped with a new high temperature ion source [1]. The mass separated In-ions were collected in a shielded counting position and analyzed γ-spectrometrically after establishment of radioactive equilibrium. The evaluation of the data is based on published decay properties [2] and took into account a correction [3] for decay of In prior to collection (average half time of volatilization: 350 ms). The corrected absolute count rates show a remarkable oscillation between a preferential feeding of high spin states (odd mass numbers) and low spin states (even mass numbers) (Fig. 1).

The yields (Y^{exp}) of the In-isotopes (sum of both isomers, respectively) (normalized to $Y(^{123}In)=0.014$ [4]) are compiled in

*Institut Laue-Langevin, Grenoble, France

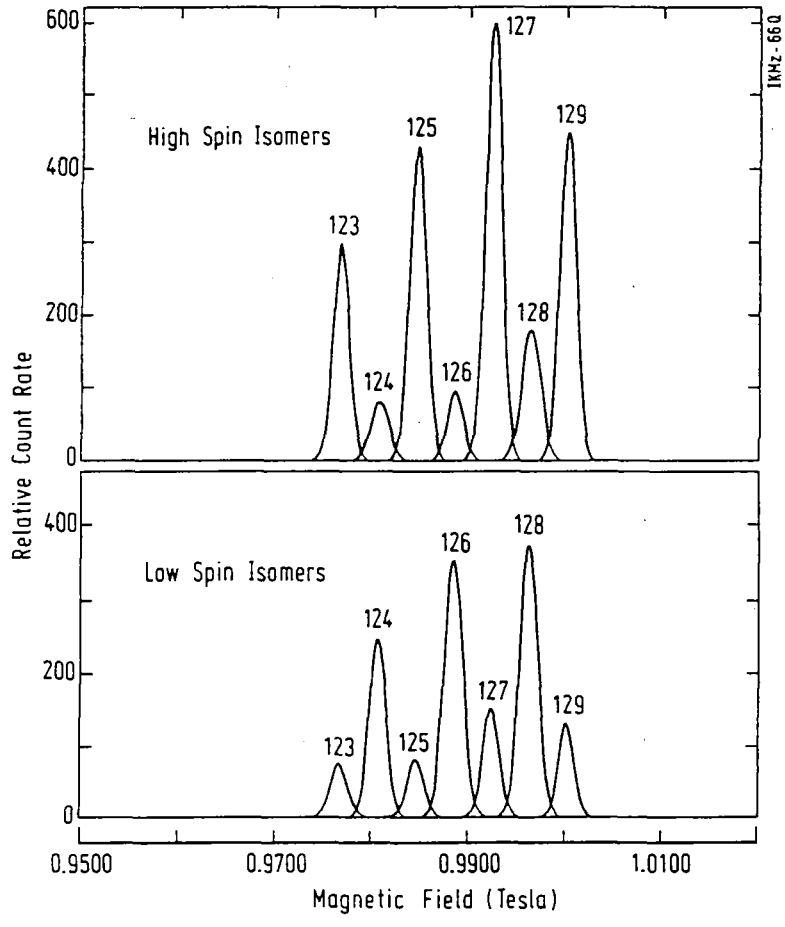

Fig. 1 Mass spectrum of high- and low-spin isomers of the In-isotopes 123-129 corrected for different detection efficiencies (peak areas = relative fission yields)

Table I. Within the error margins they agree with the corresponding values from Ref. [4] (Y[4] in Table I)

The fractions (F_H^{exp}) of high spin isomer relative to the sum yield of both isomers are also given in the table. The present technique, in principle, provides cumulative yields. In consequence, the values of F^H in chains 123, 124, and 125 may be biased by the β-decay of Cd-precursors with estimated fractional yields of 30%, 15%, and 5%, respectively (estimate based on the experimental fractional cumulative yields and a Gaußian charge dispersion with σ=0.52; EOZ=1.25, EON=1.08). In chains 126 to 129

the yields of Cd-precursors are expected to be negligible.

The values of F_H for the In-isotopes of odd mass number agree surprisingly well with the predictions according to the statistical model [5] (F_H[5] in Table I). The spins of the high spin isomers of even mass are not exactly known [2]. Therefore predictions can be made only within a band width. It appears, however, that the experimental values are considerably lower than the lowest estimate. For ^{124}In this could be due to the β-decay of the precursor. For the indium isotopes with A=126 and 128 this explanation can be excluded and at least for these two latter cases a discrepancy exists analogous to the one discussed in section 1.1 of this report.

Table I Cumulative Yields of some In-isotopes (Sum of both Isomers) Normalised to Y (^{123}In=0.014 [4]) and Values from Literature [4]. Fractions of High-spin Isomer (F_H^{exp}) from this Work and Predicted Values F_H [5]. In (): Uncertainty of Last Digit

	Y^{exp}	Y[4]	F_H^{exp}	F_H[5]
^{123}In	0.014(1)	0.014(2)	0.78(3)*	0.81
^{124}In	0.013(1)		0.26(3)*	0.47-0.64
^{125}In	0.019(1)	0.016(5)	0.84(3)*	0.81
^{126}In	0.018(1)		0.20(3)	0.47-0.59
^{127}In	0.029(1)	0.028(9)	0.80(3)	0.81
^{128}In	0.023(1)	0.015(7)	0.34(3)	0.47-0.53
^{129}In	0.022(1)		0.78(3)	0.81

*Yields of precursors (Cd) not negligible, see text.

A possible reason for the observed deviations from the expected behaviour may be a non-statistical deexcitation of the initially

highly excited fission fragments. It seems remarkable that such discrepancies are observed preferentially in odd-odd nuclei.

References

[1] J. Münzel, H. Wollnik, B. Pfeiffer and G. Jung, Nucl. Instr. Methods 186 (1981) 343

[2] Nuclear Data Sheets (Ed.: Nucl. Data Project), Academic Press

[3] J. Münzel, Dissertation, Gießen 1983

[4] T.M. Semkow, A.C. Wahl, L. Robinson, Phys. Rev. C30 (1984) 1966

[5] D.G. Madland, T.R. England, Nucl. Science and Engineering 64 (1977) 859

2. Decay Characteristics

2.1 Absolute Gamma-Ray Line Intensities and Branching Ratios in Mass Chain 133

H. Braun, H.O. Denschlag, T. Izak-Biran, W. Lauppe
A detailed report on this work has been published (cf. Radiochimica Acta 36 (1984) 95

2.2 Absolute γ-Ray Line Intensities in Mass Chains A=142-144, 146 and 147

B. Sohnius, M. Brügger, H.O. Denschlag, B. Pfeiffer
A report on this work is to be published (cf. Radiochimica Acta, in press)

INSTITUT FÜR STRAHLENPHYSIK
UNIVERSITÄT STUTTGART

1. Optical Model Analysis for Yttrium, Lanthanum and Thulium Using Neutron Differential Cross Section and Analyzing Power Data

G. Schreder, W. Grum, K.-W. Hoffmann, G. Schleußner[+], J.W. Hammer

Based on differential cross section and analyzing power measurements at E_n = 7.75 MeV at the Stuttgart SCORPION facility optical model parameters were deduced for the odd-even-nuclei ^{89}Y, ^{139}La and ^{169}Tm. Yttrium and lanthanum were treated as spherical while for the strongly deformed (β_2 = 0.31) thulium coupled channel calculations had to be applied.

Corrections for the data have been calculated for finite geometry effects and for unresolved contributions of inelastic scattering in the case of thulium. The effect of compound elastic scattering has been estimated; it had not to be corrected.

The results of the optical model analysis are given in Table I.

[+] Deceased 1983

Table I Optical Model Parameter for ^{89}Y, ^{139}La and ^{169}Tm obtained from Differential Cross Section and Analyzing Power Measurements at E_n = 7.75 MeV

Yttrium (SOM)				
V_R = 47.33 MeV	r_V = 1.24 fm	a_V = 0.62 fm	J/A = 425 MeVfm³	
W_D = 5.75 MeV	r_W = 1.26 fm	a_W = 0.58 fm	J/A = 62 MeVfm³	
V_{SO} = 7.85 MeV	r_{SO} = 1.15 fm	a_{SO} = 0.488fm		
$\beta_{2/4}$ = 0				
Lanthanum (SOM)*				
V_R = 47.21 MeV	r_V = 1.24 fm	a_V = 0.475fm	J/A = 397 MeVfm³	
W_D = 7.32 MeV	r_W = 1.20 fm	a_W = 0.58 fm	J/A = 61 MeVfm³	
V_{SO} = 7.0 MeV	r_{SO} = 1.10 fm	a_{SO} = 0.60 fm		
Thulium (CCC)				
V_R = 44.93 MeV	r_V = 1.27 fm	a_V = 0.63 fm	J/A = 416 MeVfm³	
W_D = 7.18 MeV	r_W = 1.27 fm	a_W = 0,48 fm	J/A = 51 MeVfm³	
V_{SO} = 6.0 MeV	r_{SO} = 1.07 fm	a_{SO} = 0.63 fm		
β_2 = +0.31	β_4 = +0.01			

*For better data fitting a deformation of β_2 = 0.26 only for the real potential was used in the calculations. Reasons are given in Ref. [1].

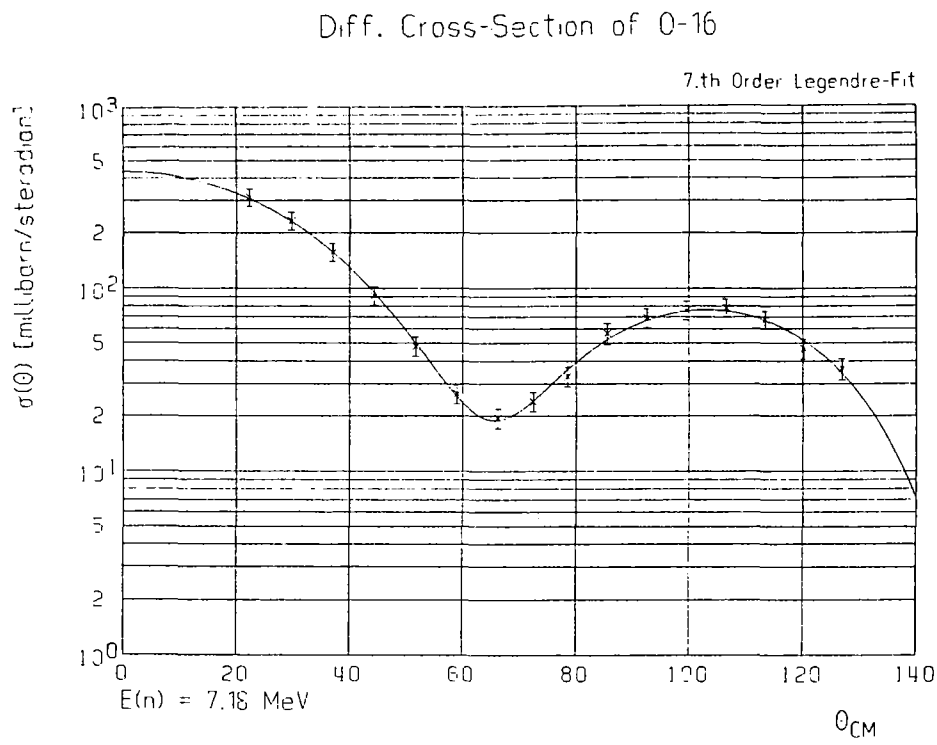

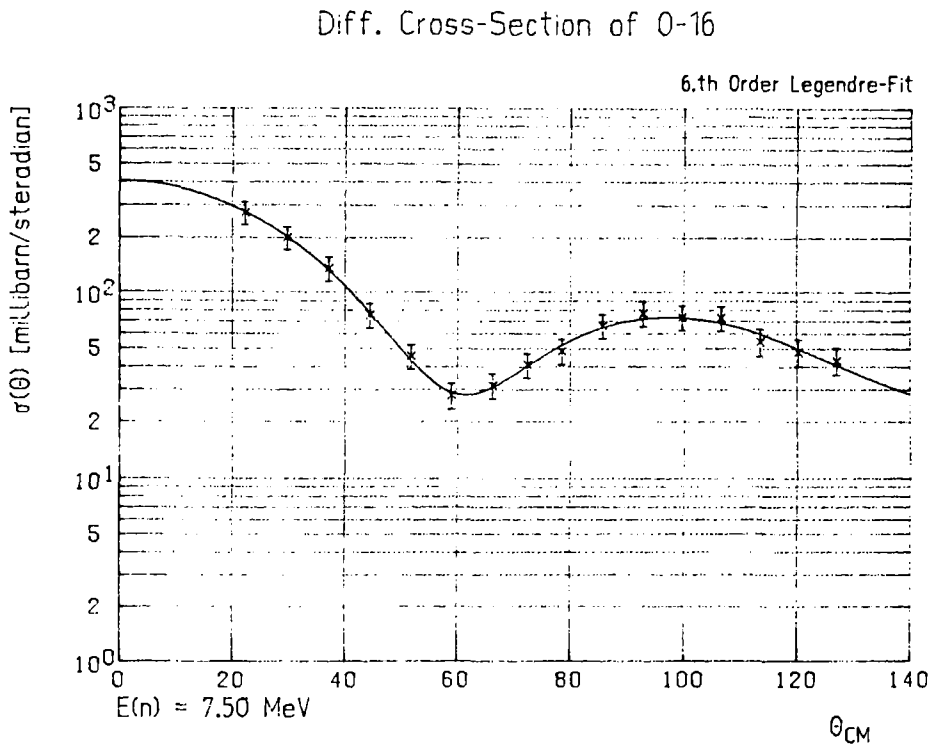

Fig. 1 Differential cross section of Oxygen-16 for neutrons of E_n = 7.18 and 7.50 MeV

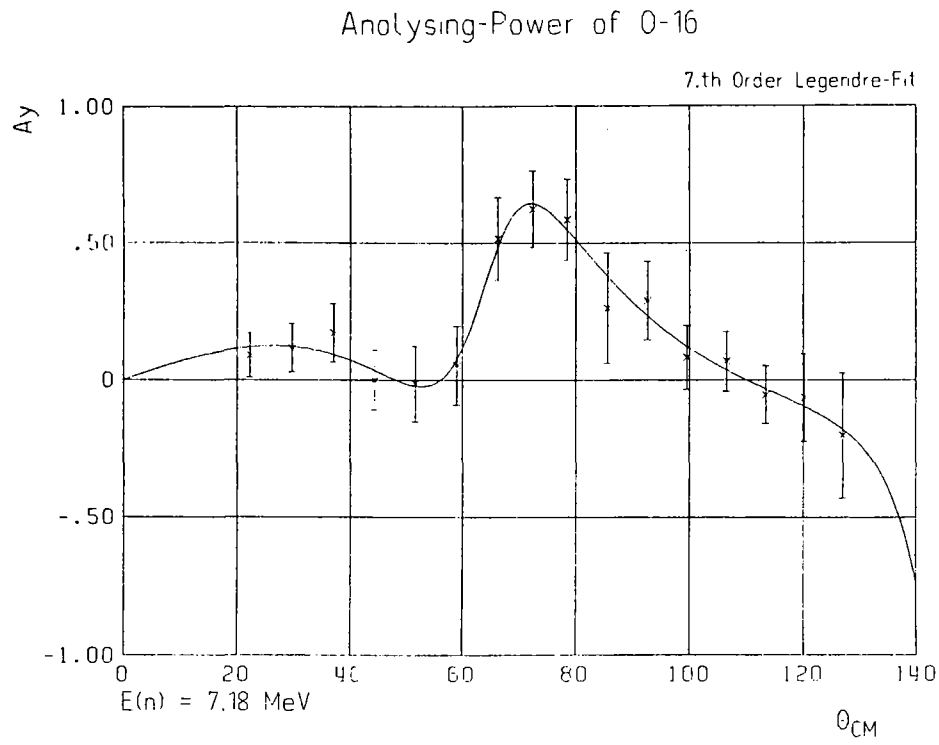

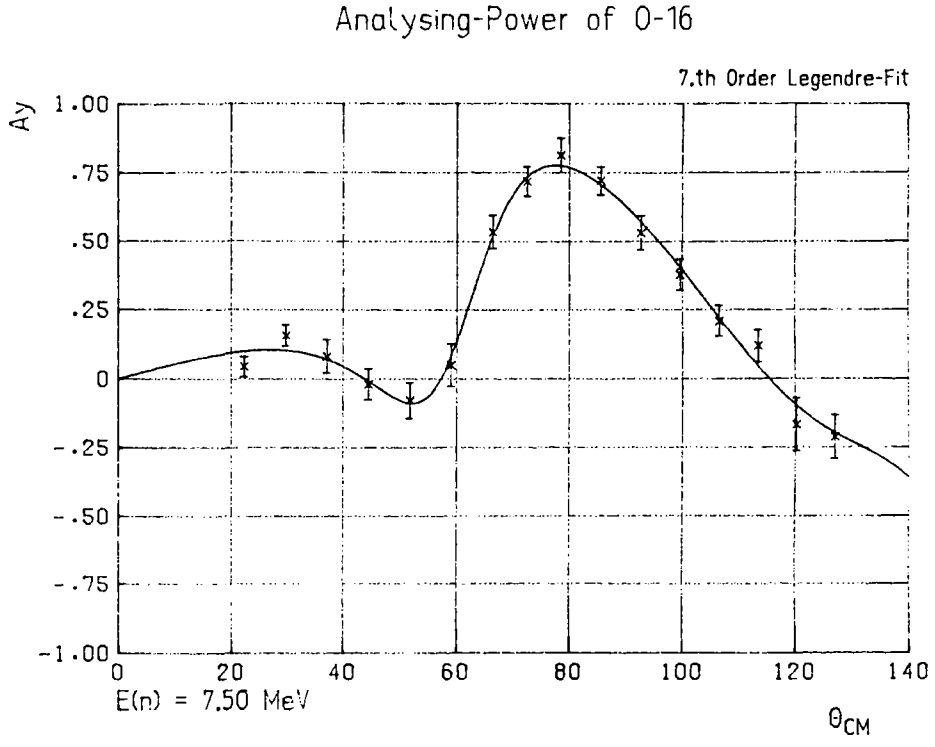

Fig. 2 Analyzing power of Oxygen-16 for neutrons of E_n = 7.18 and 7.50 MeV

2. Measurement of Analyzing Power and Differential Cross Section of Oxygen-16 for Neutrons of E_n = 7.18 - 8.05 MeV

G. Keilbach, W. Grum, K.-W. Hoffmann, G. Schreder, J.W. Hamacher

The differential cross section and the analyzing power of Oxygen-16 were measured for elastic scattered neutrons of E_n = 7.18, 7.50, 7.81 and 8.05 MeV using the Stuttgart SCORPION facility. The energy spread of the neutrons was about 40 keV. A pure liquid oxygen sample of 72 grams was contained in a thin walled (0.3 mm) stainless steel sample container suspended in vacuum. The contribution of the container had been measured carefully. All finite geometry corrections have been made using the modified code JANE [2].

Absolute cross-section values are obtained by calibration of the set up with elastic scattering measurements of hydrogen from a polyethylene sample.

Results for E_n = 7.18 and 7.50 MeV are given in Figs. 1 and 2.

Acknowledgement: The authors want to thank J. Raynal (Saclay) for delivering his code ECIS to us. We are also indebted to G. Haouat (Bruyères le Châtel) for lending us the thulium sample.

References

[1] G. Schreder, Untersuchung einiger mittelschwerer Kerne mit Hilfe des optischen Kernmodells. Diplomarbeit, Stuttgart (1984).

[2] E. Woye, Die Analysierstärke $A_y(0)$ für $^{12}C(n,n_{01})^{12}C$ im Neutronenenergiebereich von 6.8 - 17.3 MeV. Dissertation, Tübingen (1982).

REAKTORSTATION GARCHING
FACHBEREICH PHYSIK
TECHNISCHE UNIVERSITÄT MÜNCHEN

Coherent Neutron Scattering Lengths and Total Cross Sections

1. Molybdenum and its Isotopes

L. Koester, K. Knopf, W. Waschkowski

Bound coherent neutron scattering lengths b and total cross sections σ_{tot} were measured on ordinary Mo and on isotopically enriched samples. By means of Christiansen filter technique and transmission measurements with resonance activation and resonance scattering detectors we obtained the following data set (to be published):

^{ord}Mo:	b = 6.71(2) fm ,	σ_{tot}/1.26 eV = 5.954(5) b,
		σ_{tot}/5.2 eV = 5.721(15) b,
		σ_{tot}/18.8 eV = 5.35(16) b,
^{92}Mo:	b = 6.89(6) fm,	σ_{tot}/1.26 eV = 6.4(5) b,
^{94}Mo:	b = 6.77(6) fm,	" = 5.7(4) b,
^{95}Mo:	b = 7.07(5) fm,	" = 7.2(5) b,
^{96}Mo:	b = 6.18(5) fm,	" = 4.9(4) b,
^{97}Mo:	b = 7.01(7) fm,	" = 6.3(5) b,
^{98}Mo:	b = 6.57(5) fm,	" = 5.8(6) b,
^{100}Mo:	b = 6.83(5) fm,	" = 5.1(4) b.

2. Interaction of Neutrons with Zinc and its Isotopes

L. Koester, K. Knopf, W. Waschkowski, A. Klüver

Coherent neutron scattering lengths and cross sections have been measured of elemental Zn, Zn-compounds and on isotopically enriched samples for neutron energies from 0.5 meV up to 143 keV using different techniques. From the experimental data the following quantities were obtained:

- the coherent scattering lengths (b in fm) of Zn (5.689 ± 0.014); ^{64}Zn(5.23 ± 0.04); ^{66}Zn(5.98 ± 0.05); ^{67}Zn(7.58 ± 0.08; b_+ = 9.4 ± 0.5/5.8 ± 0.5; b_- = 5.0 ± 0.7/10.1 ± 0.7); ^{68}Zn(6.04 ± 0.03);

- the potential scattering radii (R´ in fm) of Zn(6.2 ± 0.2); ^{64}Zn(6.0 ± 0.3) and ^{66}Zn(6.2 ± 0.3).

- the absorption cross sections (σ_γ at 0.025 eV in barn) of Zn(1.11 ± 0.02); ^{64}Zn(1.1 ± 0.1) and ^{66}Zn(0.62 ± 0.06).

Derived quantities are the "zero energy" scattering cross sections (σ_0 in barn) for Zn(4.128 ± 0.010) and ^{67}Zn(7.8 ± 0.3) and the incoherent bound cross sections of Zn(0.061 ± 0.023) and ^{67}Zn(0.6 ± 0.4).

In the epithermal region the Zn-cross section can be described by introduction of two strong bound levels of ^{67}Zn+n for which estimated parameters are given.

Submitted to Zeitschrift für Physik A.

3. Neutron Scattering Lengths and Cross Sections of the Barium Isotopes

L. Koester, K. Knopf, W. Waschkowski

Coherent neutron scattering lengths and total cross sections have been measured for barium compounds and on isotopically enriched samples for neutron energies from 0.5 meV up to 132 eV using different techniques. From the experimental data the following quantities were obtained:

- the coherent scattering lengths (in fm) of Ba(5.07 ± 0.03) and of the isotopes with mass numbers 130(-3.6 ± 0.6); 132(7.8 ± 0.3); 134(5.7 ± 0.1); 135(4.66 ± 0.10); 136(4.90 ± 0.08); 137(6.82 ± 0.10) and 138(4.83 ± 0.08).

- the absorption cross sections σ_γ(at 0.0025 eV in barn): of Ba(1.1 ± 0.1) and of the isotopes: 130(30 ± 5); 136(0.68 ± 0.17); 137(3.6 ± 0.2) and 138(0.27 ± 0.14).

- zero-energy scattering cross sections for Ba and the isotopes 136,137 and 138.
  On the basis of these data, the isotopic- and spin-incoherent cross sections and the (s)-resonance contributions to the coherent scattering lengths have been determined and discussed.

Submitted to Zeitschrift für Physik A.

INSTITUT FÜR KERNCHEMIE
PHILIPPS-UNIVERSITÄT MARBURG

1. Gamma-Ray Catalog

U. Reus, W. Westmeier

Quantitative information on gamma rays from the decay of radioactive nuclides is required in many areas of nuclear science as well as related fields. We have therefore produced a compilation of decay properties of all known radionuclides, with the main emphasis on energies and absolute intensities of gamma rays. A first printed version of this catalog was issued in 1979, and a second edition, including references through June 1982, was completed in 1983. The latest version contains information on 2526 nuclides and isomers with a total of more than 47.000 gamma rays and X-rays, the information on X-rays accompanying radioactive decay being a newly introduced feature. The catalog is presented in two parts: In Part I gamma rays are listed in order of increasing energy for the purpose of identification of unknown gamma lines. In Part II complete data sets for each nuclide are listed in order of mass number A and nuclear charge Z of the nuclides. This part also contains additional information, references, and comments in case of any discrepancies.
The revised catalog has been published in "Atomic Data and Nuclear Data Tables", Volume 29, Nos. 1,2 (1983). Further updates of the catalog are envisaged.

2. Alpha-Energy Catalog

W. Westmeier, A. Merklin

A table of alpha-decay properties of all known alpha-emitting nuclides, which includes data on alpha energies, intensities, and the abundance of the alpha branch, is being compiled. The table is planned to be laid out in a manner similar to the Gamma-Ray Catalog.

Both tables are compiled under the auspices of the Fachinformationszentrum Energie, Physik, Mathematik GmbH (FIZ) in Karlsruhe.

PHYSIKALISCH-TECHNISCHE BUNDESANSTALT
BRAUNSCHWEIG

1. Fission Spectra and Cross Sections

1.1 Cf-252 Spectrum-Averaged Neutron Cross Sections*

W. Mannhart

Spectrum-averaged neutron cross sections measured in the well-defined Cf-252 neutron field are of some use in testing the adequacy of $\sigma(E)$ data sets which are of importance for reactor metrology purposes. Data on the reactions $^{51}V(n,p)$, $^{51}V(n,\alpha)$, $^{65}Cu(n,2n)$, $^{64}Zn(n,p)$, $^{127}I(n,2n)$ and $^{199}Hg(n,n')$ were determined. In the case of $^{65}Cu(n,2n)$ and $^{127}I(n,2n)$ no results of previous experiments were available. The measurement of $^{51}V(n,p)$ and $^{51}V(n,\alpha)$ is due to the availability of data from recent $\sigma(E)$ experiments [3,4]. The present data extend the base of high-quality Cf-252 spectrum-averaged data and were included in an evaluation of available experimental data with a complete uncertainty covariance matrix. The evaluation now comprises 35 different neutron reactions.

The experimental results are given in Table I. The data are compared with those calculated based on $\sigma(E)$ data from ENDF/B-V and from other recent sources. In the calculation two different representations of the Cf-252 neutron spectrum were used. The NBS segment-adjusted spectrum [1] and the very recent Los Alamos spectrum [2] based upon nuclear-evaporation theory.

For the reactions $^{51}V(n,\alpha)$, $^{65}Cu(n,2n)$ and $^{127}I(n,2n)$ which are all sensitive only above 8 MeV neutron energy, the Los Alamos spectrum gives substantially lower results than the NBS spectrum. This indicates a possible underestimation of the Cf-252 neutron spectrum by the Los Alamos data at high neutron energies.

---

*To be published in Proc. 5th ASTM-EURATOM Symp. Reactor Dosimetry, Geesthacht, FRG, September 1984

Table I Comparison between Experimentally Determined and Calculated Spectrum-averaged Cross Sections in the Cf-252 Neutron Field

Reaction	$\langle\sigma\rangle^{EXP}$ mb	$\langle\sigma\rangle^{CALC}$ mb		$\sigma(E)$ from:
		NBS spectrum [1]	Los Alamos spectrum [2]	
$^{51}V(n,p)$	0.637 ± 0.018	0.545 0.680	0.519 0.647	ENDF/B-V [3]
$^{51}V(n,\alpha)$	$(3.88 \pm 0.12)\times10^{-2}$	3.74×10^{-2} 3.91×10^{-2}	3.32×10^{-2} 3.48×10^{-2}	ENDF/B-V [4]
$^{65}Cu(n,2n)$	0.665 ± 0.023	0.656	0.547	ENDF/B-V
$^{64}Zn(n,p)$	41.1 ± 1.3	39.2	39.3	[5]
$^{127}I(n,2n)$	2.07 ± 0.07	2.32	1.99	ENDF/B-V
$^{199}Hg(n,n')$	295 ± 8	245	-	[6]

1.2 U-235 Spectrum-Averaged Neutron Cross Sections*

W. Mannhart, A. Fabry+

The cross sections of 17 neutron reactions were measured in a U-235 neutron field generated in a cavity inside the thermal column of the Belgian BR1 reactor at Mol. Corrections were applied for scattering, wall return and other disturbing effects to reduce the data to those of a pure U-235 neutron field. Together with similar experiments in the Cf-252 neutron field, these data are of use in the interpretation of neutron detector responses in complex reactor pressure vessel neutron fields.

The present data, shown in Table II, essentially supported the results of earlier experiments with the exception of those of high-threshold reactions where fundamental differences were found. The data were compared with calculated data based on different $\sigma(E)$ data sets and on two descriptions of the U-235 neutron spectrum. Besides the commonly accepted ENDF/B-V Watt spectrum, the theoretical Los Alamos spectrum [7] of $^{235}U + n$ (0.00 MeV) was also used.

The comparison between the experimental and calculated values shows that the Los Alamos spectrum results in a better description of the high-energy tail of the U-235 neutron spectrum compared with the ENDF/B-V Watt spectrum which underestimates this tail.

---

*To be published in Proc. 5th ASTM-EURATOM Symp. Reactor Dosimetry, Geesthacht, FRG, September 1984

+S.C.K./C.E.N., Mol, Belgium

Table II U-235 Spectrum-averaged Neutron Cross Sections

Reaction	$\langle\sigma\rangle^{EXP}$ mb	$\langle\sigma\rangle^{CALC}$ mb		$\sigma(E)$ from:
		ENDF/B-V Watt spectrum	Los Alamos spectrum	
$^{24}Mg(n,p)$	1.50 ± 0.06	1.51	1.50	[5]
$^{27}Al(n,p)$	3.95 ± 0.20	4.26	4.19	ENDF/B-V
$^{27}Al(n,\alpha)$	0.706± 0.028	0.719	0.718	ENDF/B-V
		0.686	0.685	[8]
$^{46}Ti(n,p)$	11.6 ± 0.4	11.2	11.0	ENDF/B-V
$^{47}Ti(n,p)$	17.7 ± 0.6	22.5	22.3	ENDF/B-V
$^{48}Ti(n,p)$	0.302± 0.010	0.281	0.281	ENDF/B-V
$^{51}V(n,p)$	0.503± 0.024	0.430	0.425	ENDF/B-V
		0.537	0.530	[3]
$^{51}V(n,\alpha)$	$(2.41\pm 0.09)\times10^{-2}$	2.23×10^{-2}	2.28×10^{-2}	ENDF/B-V
		2.38×10^{-2}	2.42×10^{-2}	[4]
$^{54}Fe(n,p)$	80.5 ± 2.3	81.0	80.1	ENDF/B-V
$^{56}Fe(n,p)$	1.09 ± 0.04	1.04	1.03	ENDF/B-V
$^{59}Co(n,p)$	1.41 ± 0.05	1.44	1.42	[9]
$^{59}Co(n,\alpha)$	0.161± 0.007	0.150	0.149	ENDF/B-V
$^{59}Co(n,2n)$	0.202± 0.006	0.183	0.200	ENDF/B-V
$^{58}Ni(n,2n)$	$(4.19\pm 0.22)\times10^{-3}$	2.80×10^{-3}	3.22×10^{-3}	ENDF/B-V
		3.06×10^{-3}	3.54×10^{-3}	[10]
$^{90}Zr(n,2n)$	0.103± 0.004	0.079	0.090	[5]
$^{115}In(n,n')$	190.3± 7.3	179.2	180.1	ENDF/B-V
$^{197}Au(n,2n)$	3.50 ± 0.13	3.22	3.31	ENDF/B-V

The Experimental data are compared with those calculated using two spectrum representations: (i) the ENDF/B-V Watt spectrum and (ii) the theoretical Los Alamos spectrum [7]. The $\sigma(E)$ data were mainly taken from ENDF/B-V and a few other sources.

1.3 Preliminary Evaluation of the Cf-252 Neutron Spectrum*

W. Mannhart

As the first step towards a future evaluation of the Cf-252 neutron spectrum based mainly on recent time-of-flight experiments, an evaluation has been made which considers the integral responses of diverse neutron detectors in this neutron field. The availability of these data with complete covariance matrices has been a factor in favour of the present evaluation, giving it preference over another which is at present hampered by a lack of or incomplete uncertainty information. The evaluation being a least-squares adjustment used the energy responses of 25 different neutron reactions covering the energy range between a few keV and 20 MeV in the neutron spectrum. The reactions were: $^{19}F(n,2n)$, $^{24}Mg(n,p)$, $^{27}Al(n,p)$, $^{27}Al(n,\alpha)$, $^{46}Ti(n,p)$, $^{48}Ti(n,p)$, $^{55}Mn(n,2n)$, $^{54}Fe(n,p)$, $^{56}Fe(n,p)$, $^{58}Ni(n,p)$, $^{58}Ni(n,2n)$, $^{59}Co(n,\alpha)$, $^{59}Co(n,2n)$, $^{63}Cu(n,\gamma)$, $^{63}Cu(n,\alpha)$, $^{63}Cu(n,2n)$, $^{64}Zn(n,p)$, $^{90}Zr(n,2n)$, $^{115}In(n,\gamma)$, $^{115}In(n,n')$, $^{197}Au(n,\gamma)$, $^{235}U(n,f)$, $^{237}Np(n,f)$, $^{238}U(n,f)$ and $^{239}Pu(n,f)$.

The results of the evaluation are shown in Figure 1. It is quoted relative to a spectral distribution of

$$\chi_{IN}(E) = \begin{cases} 0.6680 \quad \sqrt{E} \quad e^{-E/1.42} & 0 \le E \le 6 \text{ MeV} \\ 0.7997 \quad \sqrt{E} \quad e^{-E/1.362} & 6 \le E \le 20 \text{ MeV} \end{cases} \qquad (1)$$

This spectral distribution essentially corresponds to the NBS spectrum [1] but neglects the structure of this spectrum below 6 MeV and has been renormalized. The evaluation was carried out in energy bins of 0.5 MeV width between 0 MeV and 10 MeV and with bins of 1 MeV above 10 MeV. Figure 1 shows the ratio of the bin averages of the evaluation relative to that of eq. (1). The evaluation gave a chi-square of 19.3 corresponding to 25 degrees of freedom. The error bars shown in the figure are the square roots of the diagonal elements of the relative covariance matrix of the evaluation.

---

*To be published in Proc. IAEA Advisory Group Meeting on Nulear Standard Reference Data, Geel, Belgium, November 1984

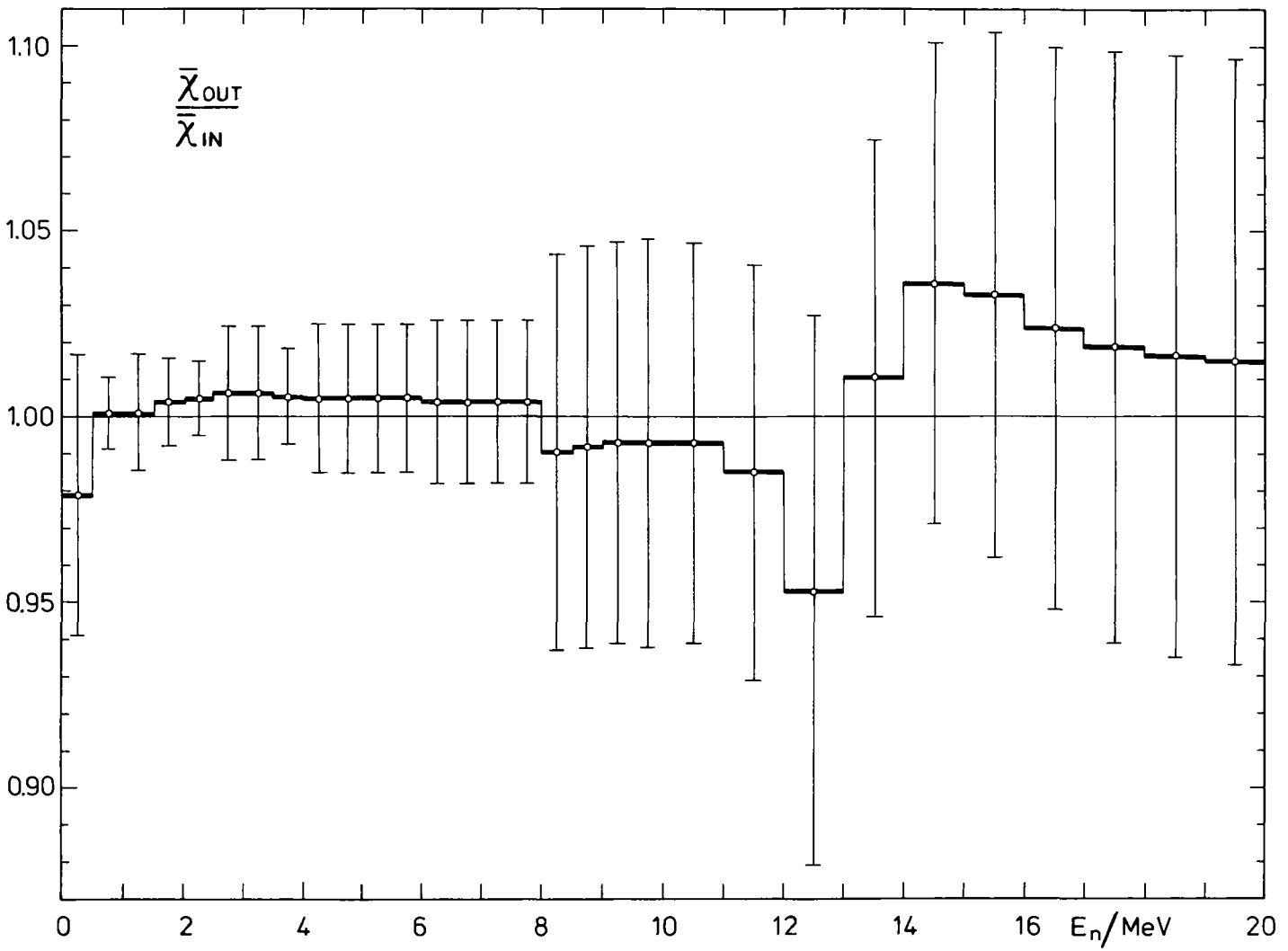

Fig. 1 Ratio of evaluated Cf-252 neutron spectrum relative to a reference spectrum (see text).

1.4 Investigation of the Shape of the Cf-252 Neutron Spectrum Above 20 MeV

W. Mannhart

A recent time-of-flight experiment indicated a strong excess of neutrons in the Cf-252 neutron spectrum above 20 MeV [11]. To validate this effect by an independent method the responses of two (n,3n) reactions which are sufficiently sensitive in this energy range were measured. The reactions were ^{107}Ag(n,3n) and ^{169}Tm(n,3n). In parallel, the (n,2n) spectrum-averaged cross-sections of both nuclides were also determined to eliminate a possible bias in the experiment. The experimental results are compared with calculations based on different assumptions on the shape of the neutron spectrum. The energy-dependent cross sections used in this comparison for the (n,2n) reactions as well as for the (n,3n) reactions were taken from the same source [12,13].

The experimental results are preliminary and require some additional corrections which have not yet been made. These corrections should not exceed the magnitude of about 30 %. Nevertheless, these preliminary results seem to be sufficient to allow some conclusions to be drawn from the summary result shown in Table III.

The results of both (n,2n) reactions which are insensitive to the portion of the neutron spectrum above 20 MeV support the NBS spectrum [1] more than a pure Maxwellian with kT = 1.42 MeV. This effect is well known from the responses of other high-threshold reactions in the Cf-252 neutron field [14]. In the case of the (n,3n) reactions the calculation was made up to 28 MeV, the upper limit of $\sigma(E)$ data available. The NBS spectrum was extrapolated in its high energy tail from 20 MeV to 28 MeV. The spectrum measured at the Technical University Dresden (TUD) follows the shape of the NBS spectrum up to 20 MeV and shows an increasing excess of neutrons between 20 MeV and 30 MeV. In the case of the TUD spectrum the response of both (n,3n) reactions extends above 28 MeV. Therefore only calculated lower limits can be quoted.

Table III Comparison of Experimentally Determined Cf-252 Spectrum-averaged Neutron Cross Sections of (n,2n) and (n,3n) Reactions with Calculated ones based on various Representations of the Neutron Spectrum

Reaction	Q-value MeV	$\langle\sigma\rangle^{EXP}$ mb	$\langle\sigma\rangle^{CALC}$ mb		
			NBS spectrum [1]	Maxwellian kT=1.42 MeV	TUD spectrum [11]
$^{169}Tm(n,2n)$	- 8.1	5.56	6.27	7.19	-
$^{107}Ag(n,2n)$	- 9.6	0.346	0.489	0.594	-
$^{169}Tm(n,3n)$	-14.9	1.72×10^{-2}	1.36×10^{-2}	1.97×10^{-2}	$> 2.74 \times 10^{-2}$
$^{107}Ag(n,3n)$	-17.5	1.12×10^{-3}	0.95×10^{-3}	1.50×10^{-3}	$> 7.61 \times 10^{-3}$

The results of both (n,3n) reactions indicate a small excess of neutrons compared with the NBS spectrum in the energy range above 20 MeV. However, the results do not confirm the magnitude of the excess of the TUD spectrum. A factor of 2.0 in the calculated data based on the TUD spectrum relative to those based on the NBS spectrum in the case of ^{169}Tm(n,3n) and even of 8.0 in the case of ^{107}Ag(n,3n) is believed to be a sound basis for the conclusions drawn.

1.5 Elastic and Inelastic Scattering of Fast Neutrons on Carbon

R. Böttger, H.J. Brede, H. Klein, H. Schölermann and B.R.L. Siebert

Scattering cross sections were measured precisely for natural carbon and polyethylene samples at neutron energies of 6.23, 7.21, 8.16, 9.16, 11.05, 11.90, 12.84 and 13.75 MeV. The experiments were performed with the multi-angle time-of-flight spectrometer specially designed for this purpose [15]. In order to determine the relevant parameters such as the mean neutron energy, the energy width and the angular resolution and to consider sample size effects, the experimental TOF spectra were compared with Monte Carlo simulations [16]. The ratios of the measured to the expected yields as calculated on the basis of evaluated cross sections (ENDF/B-V) ranged from 0.6 to 2.3 for the elastic and inelastic scattering on carbon, while the n-p scattering was reproduced within the uncertainties of 2.5 to 6 % estimated for these experiments.

Sensitivity studies showed that errors in the determination of the mean inital energies and associated density distributions, the effective scattering angles, the detection efficiencies and the sample size corrections may possibly explain some of the discrepancies between the present data set and the results of earlier experiments considered in the evaluation.

In summary we conclude from these investigations that an improved evaluation is needed before the carbon scattering cross section can be used as a reference in the energy range above 9 MeV.

References

[1] J. Grundl, C. Eisenhauer, Techn. Doc. IAEA-208, Vol. I, (1978) p. 53

[2] D.G. Madland, R.J. LaBauve, J.R. Nix, Proc. IAEA Advisory Group Meeting on Nuclear Standard Reference Data, Geel, Belgium, November 1984 (to be published)

[3] D.L. Smith, J.W. Meadows, J. Kanno, ANL-NDM-85 (1984)

[4] J. Kanno, J.W. Meadows, D.L. Smith, ANL-NDM-86 (1984)

[5] S. Tagesen, H. Vonach, B. Strohmaier, Physics Data 13-1 (1979)

[6] K. Sakurai et al., J. Nucl. Sci. Techn. 19 (1982) 775

[7] D.G. Madland, J.R. Nix, Nucl. Sci. Eng. 81 (1982) 213

[8] S. Tagesen, H. Vonach, Physics Data 13-3 (1981)

[9] D.L. Smith, J.W. Meadows, Nucl. Sci. Eng. 60 (1976) 187

[10] A. Pawlik, G. Winkler, INDC (AUS) - 9/L (1983)

[11] H. Märten, D. Seeliger, B. Stobinski, in Nuclear Data for Science and Technology, K.H. Böckhoff, Ed., D. Reidel Publ. Comp., Dordrecht, Holland (1983) p. 488

[12] B.P. Bayhurst et al., Phys. Rev. C 12 (1975) 451

[13] L.R. Veeser, E.D. Arthur, P.G. Young, Phys. Rev. C 16 (1977) 1792

[14] W. Mannhart, INDC (NDS) - 146/L (1983) p. 213

[15] R. Böttger, H.J. Brede, M. Cosack, G. Dietze, R. Jahr, H. Klein, H. Schölermann, B.R.L. Siebert, Proc. of the Intern. Conf. on Nuclear Data, Antwerp 1982, K.H. Böckhoff, Ed., Reidel Publ. Comp., Dordrecht, Holland (1983) p. 836

[16] H. Klein, B.R.L. Siebert, R. Böttger, H.J. Brede, H. Schölermann, ibid, p. 891

2. Radionuclide Data

2.1 X-ray Emission Probability of ^{93m}Nb

K. Debertin

A ^{93m}Nb solution with known activity concentration (determined by the CBNM, Geel) was used for the quantitative preparation of solid sources. The K_α and K_β X-ray emission rates of these sources were measured by means of calibrated planar germanium and Si(Li) detectors. As a result, we obtained for the emission probabilities

$$p(K_\alpha) = 0.0926 \pm 0.0015$$

$$p(K_\beta) = 0.0181 \pm 0.0004$$

$$p(K_\beta)/p(K_\alpha) = 0.195 \pm 0.004$$

FACHINFORMATIONSZENTRUM ENERGIE, PHYSIK, MATHEMATIK GMBH

Status Report

H. Behrens, P. Luksch, H.W. Müller

1. STN International

The Database "Physics Briefs" produced by the Fachinformationszentrum has been implemented on the new Network STN International established by the American Chemical Abstracts Service (CAS) and the Fachinformationszentrum, and can now be accessed via the nodes in Columbus and Karlsruhe.

2. Recent Compilations

The following new issues were published in the series Physics Data:

16-3	(1985)	The cubic Structure Types Described in their Space Groups with the Aid of Frameworks E. Hellner, H. Sowa
25-1	(1984)	Cosmic Rays on Earth O.C. Allkofer, P.K.F. Grieder
17-2	(1985)	Compilation of Experimental Values of Internal Conversion Coefficients and Ratios for Nuclei with Z 60 H.H. Hansen
5-21	(1984)	Gases and Carbon in Metals (Thermodynamic Kinetics and Properties). Part XXI: Group Ib Metals (1): Copper E. Fromm, W. Hehn, H. Jehn, G. Hörz

3. Bibliography of existing Data Compilations

The bibliographic data base "Physcomp" covering data compilation in physics on a worldwide basis has been updated. The printed version has been published in the Physics Data series.

4. The Evaluated Nuclear Structure Data File (ENSDF)

The ENSDF data file is prepared in an international network. The Karlsruhe group is responsible for the mass range A=81 to 100.

In 1984, the mass chain A=98 was published. The evaluation of the chains A=81,94, and 97 is finished; these mass chains are now in the review procedure. We started the evaluation of A=83 mass chain, while the work on A=82,93, and 99 is going on.

The online retrievable ENSDF file is updated twice a year. In 1984, 28 mass chains have been replaced by their new versions, i.e. approx. 10% of the file has been renewed. This caused the file to grow by about 10%.

The Medlist radioactive decay data, which are derived from ENSDF, are calculated and included into the MEDLIST file. About 250 radioactive decay data sets have been updated, i.e. approx. 10% of the file has been renewed, and the file has grown by about 4%.

The bibliographic data base "Nuclear Structure References" (NSR) has been updated monthly from January till November 1984. 3677 new documents (corresponding to 4.0% of the file) have been added. From November onwards the file is being updated in a 4-months' cycle.

APPENDIX I

Addresses of Contributing Laboratories

Institut für Kernphysik II
Director: Prof. Dr. A. Citron
Senior reporter: Dr. S. Cierjacks
Kernforschungszentrum Karlsruhe
Postfach 364o
75oo Karlsruhe

Institut für Kernphysik III
Director: Prof. Dr. G. Schatz
Senior reporter: Dr. F. Käppeler
Kernforschungszentrum Karlsruhe
Postfach 364o
75oo Karlsruhe

Institut für Neutronenphysik und Reaktortechnik
Direktor: Prof. Dr. G. Kessler
Senior reporter: Dr. F.H. Fröhner
Kernforschungszentrum Karlsruhe
Postfach 364o
75oo Karlsruhe

Institut für Chemie (1): Nuklearchemie
Director: Prof. Dr. G. Stöcklin
Senior reporter: Dr. S.M. Qaim
Kernforschungsanlage Jülich
Postfach 1913
517o Jülich

Institut für Kernphysik
Direktor: Prof. Dr. O.W. Schult
Senior reporter: Dr. K. Sistemich
Kernforschungsanlage Jülich
Postfach 1913
517o Jülich

Institut für Reine und Angewandte Kernphysik
Director: Prof. Dr. K.O. Thielheim
Senior reporter: Dr. H.-G. Priesmeyer
Universität Kiel, Geesthacht
Reaktorstr. 1
2o54 Geesthacht/Tesperhude

Institut für Physik
Director: Prof. Dr. W. Michaelis
Senior reporter: Dr. R. Pepelnik
GKSS-Forschungszentrum Geesthacht
2o54 Geesthacht

Institut für Kernchemie
Senior reporter: Dr. R. Michel
Universität zu Köln
Zülpicher Str. 47
5ooo Köln

Institut für Kernchemie
Director: Prof. Dr. G. Herrmann
Senior reporter: Prof. Dr. H.O. Denschlag
Universität Mainz
Fritz-Strassmann-Weg 2
65oo Mainz

Institut für Strahlenphysik
Director: Prof. Dr. K.W. Hoffmann
Senior reporter: Dr. J.W. Hammer
Universität Stuttgart
Allmandring 3
7ooo Stuttgart 8o

Fachbereich Physik der
Technischen Universität München
Abteilung E14, Forschungsreaktor
Head and senior reporter: Prof. Dr. L. Köster
8o46 Garching/München

Institut für Kernchemie
Senior reporter: Prof. Dr. P. Patzelt
Philipps-Universität Marburg
Lahnberge
355o Marburg/Lahn

Physikalisch-Technische Bundesanstalt
Abteilung 6, Atomphysik
Director: Prof. Dr. S. Wagner
Bundesallee 1oo
33oo Braunschweig

Fachinformationszentrum Energie, Physik, Mathematik
Directors: Drs. W. Rittberger, E.-O. Schulze
Senior reporter: Dr. H. Behrens
Kernforschungszentrum
7514 Eggenstein-Leopoldshafen 2

APPENDIX II

CINDA Type Index

Prepared by H. Behrens and G. Schust
FIZ Energie, Physik, Mathematik, Karlsruhe

ELEMENT S	A	QUANTITY	TYPE	ENERGY MIN	MAX	DOCUMENTATION REF	VOL	PAGE	DATE	LAB	COMMENTS
H	PLE	ELASTIC SCAT	EXPT-PROG	62+6	14+7	NEANDC(E)-262U	685			PTB	VOL.5.P.64.BOETTGER+ TOF, NDG
H	PLE	TOTAL	EXPT-PROG	62+6	14+7	NEANDC(E)-262U	685			PTB	VOL.5.P.64.BOETTGER+ TOF, NDG
LI	007	EVALUATION	EVAL-PROG	TR	15+7	NEANDC(E)-262U	685				VOL.5.P.15.GOEL+ KEDAK CURV CFD EXPT
LI	007	N,N TRITON	EVAL-PROG	TR	15+7	NEANDC(E)-262U	685				VOL.5.P.15.GOEL+ KEDAK CURV CFD EXPT
B	010	N,TRITON	EXPT-PROG	30+6	80+6	NEANDC(E)-262U	685			JUL	VOL.5.P.22.QAIM+ T EMISSION SIG.GRPH
C		ELASTIC SCAT	EXPT-PROG	62+6	14+7	NEANDC(E)-262U	685			PTB	VOL.5.P.64.BOETTGER+ TOF, NDG
C		TOTAL	EXPT-PROG	62+6	14+7	NEANDC(E)-262U	685			PTB	VOL.5.P.64.BOETTGER+ TOF, NDG
O	016	DIFF ELASTIC	EXPT-PROG	72+6		NEANDC(E)-262U	685			THS	VOL.5.P.51.KEILBACH+ SIG+ANALYS POW
O	016	DIFF ELASTIC	EXPT-PROG	75+6		NEANDC(E)-262U	685			THS	VOL.5.P.51.KEILBACH+ SIG+ANALYS POW
O	016	DIFF ELASTIC	EXPT-PROG	78+6		NEANDC(E)-262U	685			THS	VOL.5.P.51.KEILBACH+ SIG, NDG
O	016	DIFF ELASTIC	EXPT-PROG	80+6		NEANDC(E)-262U	685			THS	VOL.5.P.51.KEILBACH+ SIG, NDG
NA	023	N,ALPHA	EXPT-PROG	15+7		NEANDC(E)-262U	685			KIG	VOL.5.P.32.PEPELNIK+ ACTIVATION SIG
NA	023	N,PROTON	EXPT-PROG	15+7		NEANDC(E)-262U	685			KIG	VOL.5.P.32.PEPELNIK+ ACTIVATION SIG
MG	024	N,PROTON	EXPT-PROG	FISS		NEANDC(E)-262U	685			PTB	VOL.5.P.58.MANNHART+ SPECT-AVG SIG
MG	025	N,PROTON	EXPT-PROG	15+7		NEANDC(E)-262U	685			KIG	VOL.5.P.32.PEPELNIK+ ACTIVATION SIG
MG	026	N,ALPHA	EXPT-PROG	15+7		NEANDC(E)-262U	685			KIG	VOL.5.P.32.PEPELNIK+ ACTIVATION SIG
MG	026	N,PROTON	EXPT-PROG	15+7		NEANDC(E)-262U	685			KIG	VOL.5.P.32.PEPELNIK+ ACTIVATION SIG
AL	026	N,PROTON	EXPT-PROG	31+4		NEANDC(E)-262U	685			KFK	VOL.5.P.5.TRAUTVETTER+ SIG
AL	026	N,PROTON	EXPT-PROG	31+5		NEANDC(E)-262U	685			KFK	VOL.5.P.5.TRAUTVETTER+ SIG
AL	026	N,PROTON	EXPT-PROG	40-2		NEANDC(E)-262U	685			KFK	VOL.5.P.5.TRAUTVETTER+ SIG
AL	026	N,PROTON	EXPT-PROG	71+4		NEANDC(E)-262U	685			KFK	VOL.5.P.5.TRAUTVETTER+ SIG
AL	027	N,ALPHA	EXPT-PROG	15+7		NEANDC(E)-262U	685			KIG	VOL.5.P.32.PEPELNIK+ ACTIVATION SIG
AL	027	N,ALPHA	EXPT-PROG	FISS		NEANDC(E)-262U	685			PTB	VOL.5.P.58.MANNHART+ SPECT-AVG SIG
AL	027	N,PROTON	EXPT-PROG	15+7		NEANDC(E)-262U	685			KIG	VOL.5.P.32.PEPELNIK+ ACTIVATION SIG
AL	027	N,PROTON	EXPT-PROG	FISS		NEANDC(E)-262U	685			PTB	VOL.5.P.58.MANNHART+ SPECT-AVG SIG
SI	028	N,PROTON	EXPT-PROG	15+7		NEANDC(E)-262U	685			KIG	VOL.5.P.32.PEPELNIK+ ACTIVATION SIG
SI	029	N,PROTON	EXPT-PROG	15+7		NEANDC(E)-262U	685			KIG	VOL.5.P.32.PEPELNIK+ ACTIVATION SIG
P	031	N,HELIUM3	EXPT-PROG	15+7		NEANDC(E)-262U	685			KIG	VOL.5.P.32.PEPELNIK+ ACTIVATION SIG
CL	035	N,2N	EXPT-PROG	15+7		NEANDC(E)-262U	685			KIG	VOL.5.P.32.PEPELNIK+ ACTIVATION SIG
K	039	N,2N	EXPT-PROG	15+7		NEANDC(E)-262U	685			KIG	VOL.5.P.32.PEPELNIK+ ACTIVATION SIG
K	041	N,ALPHA	EXPT-PROG	15+7		NEANDC(E)-262U	685			KIG	VOL.5.P.32.PEPELNIK+ ACTIVATION SIG
K	041	N,PROTON	EXPT-PROG	15+7		NEANDC(E)-262U	685			KIG	VOL.5.P.32.PEPELNIK+ ACTIVATION SIG
CA	042	N,PROTON	EXPT-PROG	15+7		NEANDC(E)-262U	685			KIG	VOL.5.P.32.PEPELNIK+ ACTIVATION SIG
CA	043	N,PROTON	EXPT-PROG	15+7		NEANDC(E)-262U	685			KIG	VOL.5.P.32.PEPELNIK+ ACTIVATION SIG
CA	044	N,ALPHA	EXPT-PROG	15+7		NEANDC(E)-262U	685			KIG	VOL.5.P.32.PEPELNIK+ ACTIVATION SIG
CA	044	N,N PROTON	EXPT-PROG	15+7		NEANDC(E)-262U	685			KIG	VOL.5.P.32.PEPELNIK+ ACTIVATION SIG
CA	044	N,PROTON	EXPT-PROG	15+7		NEANDC(E)-262U	685			KIG	VOL.5.P.32.PEPELNIK+ ACTIVATION SIG
CA	046	N,GAMMA	EXPT-PROG	30+4		NEANDC(E)-262U	685			KFK	VOL.5.P.7.KAEPPELER+ MAXW AVERAGED
CA	048	N,GAMMA	EXPT-PROG	30+4		NEANDC(E)-262U	685			KFK	VOL.5.P.7.KAEPPELER+ MAXW AVERAGED
CA	048	N,2N	EXPT-PROG	15+7		NEANDC(E)-262U	685			KIG	VOL.5.P.32.PEPELNIK+ ACTIVATION SIG
SC	044	N,TRITON	EXPT-PROG	15+7		NEANDC(E)-262U	685			JUL	VOL.5.P.22.QAIM+ ISOMERIC SIG RATIO
SC	045	N,ALPHA	EXPT-PROG	15+7		NEANDC(E)-262U	685			KIG	VOL.5.P.32.PEPELNIK+ ACTIVATION SIG
SC	045	N,2N	EXPT-PROG	15+7		NEANDC(E)-262U	685			KIG	VOL.5.P.32.PEPELNIK+ ACTIVATION SIG
TI	046	N,PROTON	EXPT-PROG	15+7		NEANDC(E)-262U	685			KIG	VOL.5.P.32.PEPELNIK+ ACTIVATION SIG

ELEMENT S A	QUANTITY	TYPE	ENERGY MIN	MAX	DOCUMENTATION REF VOL PAGE DATE	LAB	COMMENTS
TI 046	N,PROTON	EXPT-PROG	FISS		NEANDC(E)-262U 685	PTB	VOL.5.P.58.MANNHART+ SPECT-AVG SIG
TI 047	N,DEUTERON	EXPT-PROG	15+7		NEANDC(E)-262U 685	KIG	VOL.5.P.32.PEPELNIK+ ACTIVATION SIG
TI 047	N,PROTON	EXPT-PROG	15+7		NEANDC(E)-262U 685	KIG	VOL.5.P.32.PEPELNIK+ ACTIVATION SIG
TI 047	N,PROTON	EXPT-PROG	FISS		NEANDC(E)-262U 685	PTB	VOL.5.P.58.MANNHART+ SPECT-AVG SIG
TI 048	N,DEUTERON	EXPT-PROG	15+7		NEANDC(E)-262U 685	KIG	VOL.5.P.32.PEPELNIK+ ACTIVATION SIG
TI 048	N,PROTON	EXPT-PROG	15+7		NEANDC(E)-262U 685	KIG	VOL.5.P.32.PEPELNIK+ ACTIVATION SIG
TI 048	N,PROTON	EXPT-PROG	FISS		NEANDC(E)-262U 685	PTB	VOL.5.P.58.MANNHART+ SPECT-AVG SIG
TI 049	N,DEUTERON	EXPT-PROG	15+7		NEANDC(E)-262U 685	KIG	VOL.5.P.32.PEPELNIK+ ACTIVATION SIG
TI 050	N,ALPHA	EXPT-PROG	15+7		NEANDC(E)-262U 685	KIG	VOL.5.P.32.PEPELNIK+ ACTIVATION SIG
TI 050	N,PROTON	EXPT-PROG	15+7		NEANDC(E)-262U 685	KIG	VOL.5.P.32.PEPELNIK+ ACTIVATION SIG
V 051	N,ALPHA	EXPT-PROG	15+7		NEANDC(E)-262U 685	KIG	VOL.5.P.32.PEPELNIK+ ACTIVATION SIG
V 051	N,ALPHA	EXPT-PROG	FISS		NEANDC(E)-262U 685	PTB	VOL.5.P.56.MANNHART. SPECT-AVG SIG
V 051	N,ALPHA	EXPT-PROG	FISS		NEANDC(E)-262U 685	PTB	VOL.5.P.58.MANNHART+ SPECT-AVG SIG
V 051	N,N ALPHA	EXPT-PROG	15+7		NEANDC(E)-262U 685	KIG	VOL.5.P.32.PEPELNIK+ ACTIVATION SIG
V 051	N,PROTON	EXPT-PROG	15+7		NEANDC(E)-262U 685	KIG	VOL.5.P.32.PEPELNIK+ ACTIVATION SIG
V 051	N,PROTON	EXPT-PROG	FISS		NEANDC(E)-262U 685	PTB	VOL.5.P.56.MANNHART. SPECT-AVG SIG
V 051	N,PROTON	EXPT-PROG	FISS		NEANDC(E)-262U 685	PTB	VOL.5.P.58.MANNHART+ SPECT-AVG SIG
V 235	FISS PROD G	EXPT-PROG	PILE		NEANDC(E)-262U 685	PTB	VOL.5.P.66.DEBERTIN. NB93,XRAY EMISS
CR 050	N,2N	EXPT-PROG	15+7		NEANDC(E)-262U 685	KIG	VOL.5.P.32.PEPELNIK+ ACTIVATION SIG
CR 052	N,PROTON	EXPT-PROG	15+7		NEANDC(E)-262U 685	KIG	VOL.5.P.32.PEPELNIK+ ACTIVATION SIG
CR 053	N,N PROTON	EXPT-PROG	15+7		NEANDC(E)-262U 685	KIG	VOL.5.P.32.PEPELNIK+ ACTIVATION SIG
CR 053	N,PROTON	EXPT-PROG	15+7		NEANDC(E)-262U 685	KIG	VOL.5.P.32.PEPELNIK+ ACTIVATION SIG
MN 052	N,TRITON	EXPT-PROG	15+7		NEANDC(E)-262U 685	JUL	VOL.5.P.22.QAIM+ ISOMERIC SIG RATIO
FE 054	N,PROTON	EXPT-PROG	FISS		NEANDC(E)-262U 685	PTB	VOL.5.P.58.MANNHART+ SPECT-AVG SIG
FE 056	N,PROTON	EXPT-PROG	FISS		NEANDC(E)-262U 685	PTB	VOL.5.P.58.MANNHART+ SPECT-AVG SIG
CO 059	N,ALPHA	EXPT-PROG	FISS		NEANDC(E)-262U 685	PTB	VOL.5.P.58.MANNHART+ SPECT-AVG SIG
CO 059	N,PROTON	EXPT-PROG	FISS		NEANDC(E)-262U 685	PTB	VOL.5.P.58.MANNHART+ SPECT-AVG SIG
CO 059	N,2N	EXPT-PROG	FISS		NEANDC(E)-262U 685	PTB	VOL.5.P.58.MANNHART+ SPECT-AVG SIG
NI	N,ALPHA	EXPT-PROG	50+6	15+7	NEANDC(E)-262U 685	JUL	VOL.5.P.24.QAIM+GRAPH,CFD OTHER DATA
NI 058	N,2N	EXPT-PROG	FISS		NEANDC(E)-262U 685	PTB	VOL.5.P.58.MANNHART+ SPECT-AVG SIG
CU 065	N,PROTON	EXPT-PROG	15+7		NEANDC(E)-262U 685	KIG	VOL.5.P.32.PEPELNIK+ ACTIVATION SIG
CU 065	N,2N	EXPT-PROG	FISS		NEANDC(E)-262U 685	PTB	VOL.5.P.56.MANNHART. SPECT-AVG SIG
ZN	THERMAL SCAT	EXPT-PROG	50-4	14+5	NEANDC(E)-262U 685	MUN	VOL.5.P.53.KOESTER+ SCAT LENGTH+SIG
ZN 064	N,PROTON	EXPT-PROG	FISS		NEANDC(E)-262U 685	PTB	VOL.5.P.56.MANNHART. SPECT-AVG SIG
ZN 064	THERMAL SCAT	EXPT-PROG	50-4	14+5	NEANDC(E)-262U 685	MUN	VOL.5.P.53.KOESTER+ SCAT LENGTH+SIG
ZN 066	THERMAL SCAT	EXPT-PROG	50-4	14+5	NEANDC(E)-262U 685	MUN	VOL.5.P.53.KOESTER+ SCAT LENGTH+SIG
ZN 067	THERMAL SCAT	EXPT-PROG	50-4	14+5	NEANDC(E)-262U 685	MUN	VOL.5.P.53.KOESTER+ SCAT LENGTH+SIG
ZN 068	N,PROTON	EXPT-PROG	15+7		NEANDC(E)-262U 685	KIG	VOL.5.P.32.PEPELNIK+ ACTIVATION SIG
ZN 068	THERMAL SCAT	EXPT-PROG	50-4	14+5	NEANDC(E)-262U 685	MUN	VOL.5.P.53.KOESTER+ SCAT LENGTH+SIG
ZN 070	N,PROTON	EXPT-PROG	15+7		NEANDC(E)-262U 685	KIG	VOL.5.P.32.PEPELNIK+ ACTIVATION SIG
GE 070	N,GAMMA	EXPT-PROG	30+4		NEANDC(E)-262U 685	KFK	VOL.5.P.8.WALTER+ MAXWELL AVERAGED
KR 078	N,GAMMA	EXPT-PROG	30+4		NEANDC(E)-262U 685	KFK	VOL.5.P.9.WALTER+ MAXW AVG,CFD CALC
KR 079	N,GAMMA	THEO-PROG	30+4		NEANDC(E)-262U 685	KFK	VOL.5.P.9.WALTER+ MAXW AVG
KR 080	N,GAMMA	EXPT-PROG	30+4		NEANDC(E)-262U 685	KFK	VOL.5.P.9.WALTER+ MAXW AVG,CFD CALC

ELEMENT S A	QUANTITY	TYPE	ENERGY MIN	MAX	DOCUMENTATION REF VOL PAGE DATE	LAB	COMMENTS
KR 081	N,GAMMA	THEO-PROG	30+4		NEANDC(E)-262U 685	KFK	VOL.5.P.9.WALTER+ MAXW AVG
KR 082	N,GAMMA	EXPT-PROG	30+4		NEANDC(E)-262U 685	KFK	VOL.5.P.9.WALTER+ MAXW AVG,CFD CALC
KR 083	N,GAMMA	EXPT-PROG	30+4		NEANDC(E)-262U 685	KFK	VOL.5.P.9.WALTER+ MAXW AVG,CFD CALC
KR 084	N,GAMMA	EXPT-PROG	30+4		NEANDC(E)-262U 685	KFK	VOL.5.P.9.WALTER+ MAXW AVG,CFD CALC
KR 085	N,GAMMA	THEO-PROG	30+4		NEANDC(E)-262U 685	KFK	VOL.5.P.9.WALTER+ MAXW AVG
KR 086	N,GAMMA	EXPT-PROG	30+4		NEANDC(E)-262U 685	KFK	VOL.5.P.9.WALTER+ MAXW AVG,CFD CALC
RB 085	N,ALPHA	EXPT-PROG	15+7		NEANDC(E)-262U 685	KIG	VOL.5.P.32.PEPELNIK+ ACTIVATION SIG
RB 085	N,PROTON	EXPT-PROG	15+7		NEANDC(E)-262U 685	KIG	VOL.5.P.32.PEPELNIK+ ACTIVATION SIG
RB 085	N,2N	EXPT-PROG	15+7		NEANDC(E)-262U 685	KIG	VOL.5.P.32.PEPELNIK+ ACTIVATION SIG
RB 086	N,TRITON	EXPT-PROG	15+7		NEANDC(E)-262U 685	JUL	VOL.5.P.22.QAIM+ ISOMERIC SIG RATIO
RB 087	N,PROTON	EXPT-PROG	15+7		NEANDC(E)-262U 685	KIG	VOL.5.P.32.PEPELNIK+ ACTIVATION SIG
RB 087	N,2N	EXPT-PROG	15+7		NEANDC(E)-262U 685	KIG	VOL.5.P.32.PEPELNIK+ ACTIVATION SIG
SR 084	N,GAMMA	EXPT-PROG	15+7		NEANDC(E)-262U 685	KIG	VOL.5.P.32.PEPELNIK+ ACTIVATION SIG
SR 086	N,GAMMA	EXPT-PROG	30+4		NEANDC(E)-262U 685	KFK	VOL.5.P.8.WALTER+ MAXWELL AVERAGED
SR 086	N,GAMMA	EXPT-PROG	15+7		NEANDC(E)-262U 685	KIG	VOL.5.P.32.PEPELNIK+ ACTIVATION SIG
SR 086	N,2N	EXPT-PROG	15+7		NEANDC(E)-262U 685	KIG	VOL.5.P.32.PEPELNIK+ ACTIVATION SIG
SR 087	N,GAMMA	EXPT-PROG	30+4		NEANDC(E)-262U 685	KFK	VOL.5.P.8.WALTER+ MAXWELL AVERAGED
SR 088	N,ALPHA	EXPT-PROG	15+7		NEANDC(E)-262U 685	KIG	VOL.5.P.32.PEPELNIK+ ACTIVATION SIG
SR 088	N,2N	EXPT-PROG	15+7		NEANDC(E)-262U 685	KIG	VOL.5.P.32.PEPELNIK+ ACTIVATION SIG
Y 089	DIFF ELASTIC	EXPT-PROG	78+6		NEANDC(E)-262U 685	THS	VOL.5.P.47.SCHREDER+ OPTMDL PARAMS
ZR 090	N,ALPHA	EXPT-PROG	15+7		NEANDC(E)-262U 685	KIG	VOL.5.P.32.PEPELNIK+ ACTIVATION SIG
ZR 090	N,PROTON	EXPT-PROG	15+7		NEANDC(E)-262U 685	KIG	VOL.5.P.32.PEPELNIK+ ACTIVATION SIG
ZR 090	N,2N	EXPT-PROG	15+7		NEANDC(E)-262U 685	KIG	VOL.5.P.32.PEPELNIK+ ACTIVATION SIG
ZR 090	N,2N	EXPT-PROG	FISS		NEANDC(E)-262U 685	PTB	VOL.5.P.58.MANNHART+ SPECT-AVG SIG
ZR 091	N,N PROTON	EXPT-PROG	15+7		NEANDC(E)-262U 685	KIG	VOL.5.P.32.PEPELNIK+ ACTIVATION SIG
ZR 091	N,PROTON	EXPT-PROG	15+7		NEANDC(E)-262U 685	KIG	VOL.5.P.32.PEPELNIK+ ACTIVATION SIG
ZR 092	N,PROTON	EXPT-PROG	15+7		NEANDC(E)-262U 685	KIG	VOL.5.P.32.PEPELNIK+ ACTIVATION SIG
ZR 094	N,ALPHA	EXPT-PROG	15+7		NEANDC(E)-262U 685	KIG	VOL.5.P.32.PEPELNIK+ ACTIVATION SIG
ZR 094	N,PROTON	EXPT-PROG	15+7		NEANDC(E)-262U 685	KIG	VOL.5.P.32.PEPELNIK+ ACTIVATION SIG
ZR 096	N,GAMMA	EXPT-PROG	15+7		NEANDC(E)-262U 685	KIG	VOL.5.P.32.PEPELNIK+ ACTIVATION SIG
ZR 096	N,2N	EXPT-PROG	15+7		NEANDC(E)-262U 685	KIG	VOL.5.P.32.PEPELNIK+ ACTIVATION SIG
NB 093	N,ALPHA	EXPT-PROG	15+7		NEANDC(E)-262U 685	KIG	VOL.5.P.32.PEPELNIK+ ACTIVATION SIG
NB 093	N,N ALPHA	EXPT-PROG	15+7		NEANDC(E)-262U 685	KIG	VOL.5.P.32.PEPELNIK+ ACTIVATION SIG
NB 093	N,2N	EXPT-PROG	15+7		NEANDC(E)-262U 685	KIG	VOL.5.P.32.PEPELNIK+ ACTIVATION SIG
MO	N,ALPHA	EXPT-PROG	50+6	15+7	NEANDC(E)-262U 685	JUL	VOL.5.P.24.QAIM+GRAPH,CFD OTHER DATA
MO	THERMAL SCAT	EXPT-PROG	13+0		NEANDC(E)-262U 685	MUN	VOL.5.P.52.KOESTER+ SCAT LENGTH+SIG
MO 092	N,ALPHA	EXPT-PROG	15+7		NEANDC(E)-262U 685	KIG	VOL.5.P.32.PEPELNIK+ ACTIVATION SIG
MO 092	N,PROTON	EXPT-PROG	15+7		NEANDC(E)-262U 685	KIG	VOL.5.P.32.PEPELNIK+ ACTIVATION SIG
MO 092	N,2N	EXPT-PROG	15+7		NEANDC(E)-262U 685	KIG	VOL.5.P.32.PEPELNIK+ ACTIVATION SIG
MO 092	THERMAL SCAT	EXPT-PROG	13+0		NEANDC(E)-262U 685	MUN	VOL.5.P.52.KOESTER+ SCAT LENGTH+SIG
MO 094	THERMAL SCAT	EXPT-PROG	13+0		NEANDC(E)-262U 685	MUN	VOL.5.P.52.KOESTER+ SCAT LENGTH+SIG
MO 095	THERMAL SCAT	EXPT-PROG	13+0		NEANDC(E)-262U 685	MUN	VOL.5.P.52.KOESTER+ SCAT LENGTH+SIG
MO 096	N,PROTON	EXPT-PROG	15+7		NEANDC(E)-262U 685	KIG	VOL.5.P.32.PEPELNIK+ ACTIVATION SIG
MO 096	THERMAL SCAT	EXPT-PROG	13+0		NEANDC(E)-262U 685	MUN	VOL.5.P.52.KOESTER+ SCAT LENGTH+SIG

ELEMENT S A	QUANTITY	TYPE	ENERGY MIN	MAX	DOCUMENTATION REF VOL PAGE DATE	LAB	COMMENTS
MO 097	N,PROTON	EXPT-PROG	15+7		NEANDC(E)-262U 685	KIG	VOL.5.P.32.PEPELNIK+ ACTIVATION SIG
MO 097	THERMAL SCAT	EXPT-PROG	13+0		NEANDC(E)-262U 685	MUN	VOL.5.P.52.KOESTER+ SCAT LENGTH+SIG
MO 098	N,PROTON	EXPT-PROG	15+7		NEANDC(E)-262U 685	KIG	VOL.5.P.32.PEPELNIK+ ACTIVATION SIG
MO 098	THERMAL SCAT	EXPT-PROG	13+0		NEANDC(E)-262U 685	MUN	VOL.5.P.52.KOESTER+ SCAT LENGTH+SIG
MO 100	THERMAL SCAT	EXPT-PROG	13+0		NEANDC(E)-262U 685	MUN	VOL.5.P.52.KOESTER+ SCAT LENGTH+SIG
AG 104	N,TRITON	EXPT-PROG	15+7		NEANDC(E)-262U 685	JUL	VOL.5.P.22.QAIM+ ISOMERIC SIG RATIO
AG 107	N,XN	EXPT-PROG	FISS		NEANDC(E)-262U 685	PTB	VOL.5.P.62.MANNHART.SPEC-AVG N3N SIG
AG 107	N,2N	EXPT-PROG	FISS		NEANDC(E)-262U 685	PTB	VOL.5.P.62.MANNHART. SPECT-AVG SIG
CD 110	N,PROTON	EXPT-PROG	15+7		NEANDC(E)-262U 685	KIG	VOL.5.P.32.PEPELNIK+ ACTIVATION SIG
CD 111	N,PROTON	EXPT-PROG	15+7		NEANDC(E)-262U 685	KIG	VOL.5.P.32.PEPELNIK+ ACTIVATION SIG
CD 111	TOTAL	EXPT-PROG	15+7		NEANDC(E)-262U 685	KIG	VOL.5.P.32.PEPELNIK+ ACTIVATION SIG
CD 114	N,PROTON	EXPT-PROG	15+7		NEANDC(E)-262U 685	KIG	VOL.5.P.32.PEPELNIK+ ACTIVATION SIG
CD 116	N,PROTON	EXPT-PROG	15+7		NEANDC(E)-262U 685	KIG	VOL.5.P.32.PEPELNIK+ ACTIVATION SIG
IN 110	N,TRITON	EXPT-PROG	15+7		NEANDC(E)-262U 685	JUL	VOL.5.P.22.QAIM+ ISOMERIC SIG RATIO
IN 115	N,ALPHA	EXPT-PROG	15+7		NEANDC(E)-262U 685	KIG	VOL.5.P.32.PEPELNIK+ ACTIVATION SIG
IN 115	TOTAL	EXPT-PROG	15+7		NEANDC(E)-262U 685	KIG	VOL.5.P.32.PEPELNIK+ ACTIVATION SIG
IN 115	TOTAL	EXPT-PROG	FISS		NEANDC(E)-262U 685	PTB	VOL.5.P.58.MANNHART+ SPECT-AVG SIG
IN 127	N,2N	EXPT-PROG	15+7		NEANDC(E)-262U 685	KIG	VOL.5.P.32.PEPELNIK+ ACTIVATION SIG
SB 121	N,2N	EXPT-PROG	15+7		NEANDC(E)-262U 685	KIG	VOL.5.P.32.PEPELNIK+ ACTIVATION SIG
I 127	N,2N	EXPT-PROG	FISS		NEANDC(E)-262U 685	PTB	VOL.5.P.56.MANNHART. SPECT-AVG SIG
BA	THERMAL SCAT	EXPT-PROG	50-4	13+2	NEANDC(E)-262U 685	MUN	VOL.5.P.54.KOESTER+ SCAT LENGTH+SIG
BA 130	TLS	EXPT-PROG	50-4	13+2	NEANDC(E)-262U 685	MUN	VOL.5.P.54.KOESTER+ SCAT LENGTH+SIG
BA 132	N,2N	EXPT-PROG	15+7		NEANDC(E)-262U 685	KIG	VOL.5.P.32.PEPELNIK+ ACTIVATION SIG
BA 132	THERMAL SCAT	EXPT-PROG	50-4	13+2	NEANDC(E)-262U 685	MUN	VOL.5.P.54.KOESTER+ SCAT LENGTH+SIG
BA 134	N,2N	EXPT-PROG	15+7		NEANDC(E)-262U 685	KIG	VOL.5.P.32.PEPELNIK+ ACTIVATION SIG
BA 134	THERMAL SCAT	EXPT-PROG	50-4	13+2	NEANDC(E)-262U 685	MUN	VOL.5.P.54.KOESTER+ SCAT LENGTH+SIG
BA 135	THERMAL SCAT	EXPT-PROG	50-4	13+2	NEANDC(E)-262U 685	MUN	VOL.5.P.54.KOESTER+ SCAT LENGTH+SIG
BA 136	N,PROTON	EXPT-PROG	15+7		NEANDC(E)-262U 685	KIG	VOL.5.P.32.PEPELNIK+ ACTIVATION SIG
BA 136	N,2N	EXPT-PROG	15+7		NEANDC(E)-262U 685	KIG	VOL.5.P.32.PEPELNIK+ ACTIVATION SIG
BA 136	TOTAL	EXPT-PROG	15+7		NEANDC(E)-262U 685	KIG	VOL.5.P.32.PEPELNIK+ ACTIVATION SIG
BA 136	THERMAL SCAT	EXPT-PROG	50-4	13+2	NEANDC(E)-262U 685	MUN	VOL.5.P.54.KOESTER+ SCAT LENGTH+SIG
BA 137	TOTAL	EXPT-PROG	15+7		NEANDC(E)-262U 685	KIG	VOL.5.P.32.PEPELNIK+ ACTIVATION SIG
BA 137	THERMAL SCAT	EXPT-PROG	50-4	13+2	NEANDC(E)-262U 685	MUN	VOL.5.P.54.KOESTER+ SCAT LENGTH+SIG
BA 138	N,ALPHA	EXPT-PROG	15+7		NEANDC(E)-262U 685	KIG	VOL.5.P.32.PEPELNIK+ ACTIVATION SIG
BA 138	N,GAMMA	EXPT-PROG	15+7		NEANDC(E)-262U 685	KIG	VOL.5.P.32.PEPELNIK+ ACTIVATION SIG
BA 138	N,PROTON	EXPT-PROG	15+7		NEANDC(E)-262U 685	KIG	VOL.5.P.32.PEPELNIK+ ACTIVATION SIG
BA 138	N,2N	EXPT-PROG	15+7		NEANDC(E)-262U 685	KIG	VOL.5.P.32.PEPELNIK+ ACTIVATION SIG
BA 138	THERMAL SCAT	EXPT-PROG	50-4	13+2	NEANDC(E)-262U 685	MUN	VOL.5.P.54.KOESTER+ SCAT LENGTH+SIG
LA 139	DIFF ELASTIC	EXPT-PROG	78+6		NEANDC(E)-262U 685	THS	VOL.5.P.47.SCHREDER+ OPTMDL PARAMS
CE 139	N,TRITON	EXPT-PROG	15+7		NEANDC(E)-262U 685	JUL	VOL.5.P.22.QAIM+ ISOMERIC SIG RATIO
SM 148	N,GAMMA	EXPT-PROG	30+4		NEANDC(E)-262U 685	KFK	VOL.5.P.10.WINTERS+ MAXWELL AVERAGED
SM 149	N,GAMMA	EXPT-PROG	30+4		NEANDC(E)-262U 685	KFK	VOL.5.P.10.WINTERS+ MAXWELL AVERAGED

ELEMENT S A	QUANTITY	TYPE	ENERGY MIN	MAX	DOCUMENTATION REF	VOL	PAGE	DATE	LAB	COMMENTS
SM 150	N,GAMMA	EXPT-PROG	30+4		NEANDC(E)-262U	685			KFK	VOL.5.P.10.WINTERS+ MAXWELL AVERAGED
DY 160	N,GAMMA	EXPT-PROG	NDG		NEANDC(E)-262U	685				VOL.5.P.11.BEER+ ABST,NDG
DY 161	N,GAMMA	EXPT-PROG	NDG		NEANDC(E)-262U	685				VOL.5.P.11.BEER+ ABST,NDG
DY 161	RESON PARAMS	EXPT-PROG	54 0		NEANDC(E)-262U	685			KIG	VOL.5.P.29.PRIESMEYER+ DY-162 RESPAR
DY 163	N,GAMMA	EXPT-PROG	30+4		NEANDC(E)-262U	685				VOL.5.P.12.BEER+ MAXWELL AVERAGE
ER 164	N,GAMMA	EXPT-PROG	30+4		NEANDC(E)-262U	685				VOL.5.P.12.BEER+ MAXWELL AVERAGE
TM 169	DIFF ELASTIC	EXPT-PROG	78+6		NEANDC(E)-262U	685			THS	VOL.5.P.47.SCHREDER+ OPTMDL PARAMS
TM 169	N,XN	EXPT-PROG	FISS		NEANDC(E)-262U	685			PTB	VOL.5.P.62.MANNHART.SPEC-AVG N3N SIG
TM 169	N,2N	EXPT-PROG	FISS		NEANDC(E)-262U	685			PTB	VOL.5.P.62.MANNHART. SPECT-AVG SIG
YB 170	N,GAMMA	EXPT-PROG	NDG		NEANDC(E)-262U	685				VOL.5.P.11.BEER+ ABST,NDG
YB 171	N,GAMMA	EXPT-PROG	NDG		NEANDC(E)-262U	685				VOL.5.P.11.BEER+ ABST,NDG
LU 175	N,GAMMA	EXPT-PROG	NDG		NEANDC(E)-262U	685				VOL.5.P.11.BEER+ ABST,NDG
LU 176	N,GAMMA	EXPT-PROG	NDG		NEANDC(E)-262U	685				VOL.5.P.11.BEER+ ABST,NDG
HF 176	N,GAMMA	EXPT-PROG	NDG		NEANDC(E)-262U	685				VOL.5.P.11.BEER+ ABST,NDG
HF 177	N,GAMMA	EXPT-PROG	NDG		NEANDC(E)-262U	685				VOL.5.P.11.BEER+ ABST,NDG
AU 197	N,2N	EXPT-PROG	FISS		NEANDC(3)-262U	685			PTB	VOL.5.P.58.MANNHART+ SPECT-AVG SIG
HG 198	N,GAMMA	EXPT-PROG	26+3	50+5	NEANDC(E)-262U	685				VOL.5.P.12.BEER+ ABST,NDG
HG 199	N,GAMMA	EXPT-PROG	26+3	50+5	NEANDC(E)-262U	685				VOL.5.P.12.BEER+ ABST,NDG
HG 199	TOTAL	EXPT-PROG	FISS		NEANDC(E)-262U	685			PTB	VOL.5.P.56.MANNHART. SPECT-AVG SIG
HG 200	N,GAMMA	EXPT-PROG	26+3	50+5	NEANDC(E)-262U	685				VOL.5.P.12.BEER+ ABST,NDG
HG 201	N,GAMMA	EXPT-PROG	26+3	50+5	NEANDC(E)-262U	685				VOL.5.P.12.BEER+ ABST,NDG
HG 202	N,GAMMA	EXPT-PROG	26+3	50+5	NEANDC(E)-262U	685				VOL.5.P.12.BEER+ ABST,NDG
HG 204	N,GAMMA	EXPT-PROG	26+3	50+5	NEANDC(E)-262U	685				VOL.5.P.12.BEER+ ABST,NDG
PB 204	N,2N	EXPT-PROG	15+7		NEANDC(E)-262U	685			KIG	VOL.5.P.32.PEPELNIK+ ACTIVATION SIG
U 235	FISS PROD G	EXPT-PROG	PILE		NEANDC(E)-262U	685			MNZ	VOL.5.P.46.BRAUN+ INTENSIT,A=133,NDG
U 235	FISS PROD G	EXPT-PROG	PILE		NEANDC(E)-262U	685			MNZ	VOL.5.P.46.SOHNIUS+ A=142-147,NDG
U 235	FRAG SPECTRA	EXPT-PROG	PILE		NEANDC(E)-262U	685			MNZ	VOL.5.P.41.DENSCHLAG+ Y-96,97,98 EN
U 235	FISS YIELD	EXPT-PROG	PILE		NEANDC(E)-262U	685			JUL	VOL.5.P.27.LHERSONNEAU+ Y-97
U 235	FISS YIELD	EXPT-PROG	PILE		NEANDC(E)-262U	685			MNZ	VOL.5.P.41.DENSCHLAG+ Y-96,Y-97,Y-98
U 235	FISS YIELD	EXPT-PROG	PILE		NEANDC(E)-262U	685			MNZ	VOL.5.P.43.HOERNER+ IN 123-129
U 238	N,2N	EXPT-PROG	15+7		NEANDC(E)-262U	685			KIG	VOL.5.P.32.PEPELNIK+ ACTIVATION SIG